(2)

GA-A20346

HIGH-TEMPERATURE CERAMIC SUPERCONDUCTORS

FOR PERIOD
OCTOBER 1, 1989 TO SEPTEMBER 30, 1990

ANNUAL REPORT

Prepared for
OFFICE OF NAVAL RESEARCH
800 NORTH QUINCY STREET
ARLINGTON, VIRGINIA 22217-5000

DARPA/ONR CONTRACT N00014-88-C-0714

APPROVED FOR PUBLIC RELEASE

Prepared by
K.S. MAZDIYASNI, PROGRAM MANAGER

A. CHEN
K.C. CHEN
D.M. DUGGAN
M.B. MAPLE (UCSD)
J. McKITTRICK (UCSD)
F.C. MONTGOMERY
S.S. PAK
L. PAULIUS (UCSD)
P.K. TSAI (UCSD)

APPROVED BY: T.D. Gulden
T.D. GULDEN
DIRECTOR, DEFENSE MATERIALS

GENERAL ATOMICS

SECURITY CLASSIFICATION OF THIS PAGE

REPORT DOCUMENTATION PAGE

Form Approved
OMB No. 0704-0188

1a. REPORT SECURITY CLASSIFICATION Unclassified	1b. RESTRICTIVE MARKINGS
2a. SECURITY CLASSIFICATION AUTHORITY	3. DISTRIBUTION/AVAILABILITY OF REPORT Unlimited
2b. DECLASSIFICATION/DOWNGRADING SCHEDULE	
4. PERFORMING ORGANIZATION REPORT NUMBER(S) GA-A20346 Project 3850	5. MONITORING ORGANIZATION REPORT NUMBER(S)
6a. NAME OF PERFORMING ORGANIZATION General Atomics 6b. OFFICE SYMBOL (If applicable)	7a. NAME OF MONITORING ORGANIZATION Office of Naval Research
6c. ADDRESS (City, State, and ZIP Code) P. O. Box 85608 San Diego, CA 92138	7b. ADDRESS (City, State, and ZIP Code) 800 North Quincy Avenue Arlington, VA 22217
8a. NAME OF FUNDING/SPONSORING ORGANIZATION Defense Advanced Research Agency 8b. OFFICE SYMBOL (If applicable) DARPA	9. PROCUREMENT INSTRUMENT IDENTIFICATION NUMBER N00014-88-C-0714
8c. ADDRESS (City, State, and ZIP Code) 1400 Wilson Blvd. Arlington, VA 22209	10. SOURCE OF FUNDING NUMBERS PROGRAM ELEMENT NO. / PROJECT NO. / TASK NO. / WORK UNIT ACCESSION NO.
11. TITLE (Include Security Classification) High Temperature Ceramic Superconductors	
12. PERSONAL AUTHOR(S) K. S. Mazdiyasni	
13a. TYPE OF REPORT Annual Report 13b. TIME COVERED FROM 10/1/89 TO 9/30/90	14. DATE OF REPORT (Year, Month, Day) November 15, 1990 15. PAGE COUNT
16. SUPPLEMENTARY NOTATION	

17. COSATI CODES			18. SUBJECT TERMS (Continue on reverse if necessary and identify by block number)		
FIELD	GROUP	SUB-GROUP	Sol-Gel	Thick film	Thin film
			Precursor Compounds	Fiber	Electromagnetic properties
			Processing	Flux Creep	Microstructures

19. ABSTRACT (Continue on reverse if necessary and identify by block number)

The principal goals of this program are (1) to demonstrate fabrication of high-temperature ceramic superconductors via sol-gel method that can operate at or above 90K with appropriate current density, J_c, in forms useful for application in resonant cavities, magnets, motors, sensors, computers, and other devices; and (2) to fabricate and demonstrate selected components made of these materials, including microwave cavities and magnetic shields. Chemical pathways for synthesis of 123 identified, process parameters window for sol-gel derived 123 fibers established, continuous flexible fibers 15-200 μm in diameter producted, fibers with T_c ~92.5 K, ΔT=1.5 K, J_c = 2 x 10^3 A/cm^2 at 77 K, 0 field; 4 x 10^3 at 57K, 100 Oe was produced, formed adherent 123 oriented films on metals and ceramic substrates, achieved film T_c ~92 K, ΔT = 4 K, J_c = 400 A/cm^2 at 40 K, 0 field.

20. DISTRIBUTION/AVAILABILITY OF ABSTRACT ☒ UNCLASSIFIED/UNLIMITED ☐ SAME AS RPT. ☐ DTIC USERS	21. ABSTRACT SECURITY CLASSIFICATION
22a. NAME OF RESPONSIBLE INDIVIDUAL Dr. Wallace Arden Smith	22b. TELEPHONE (Include Area Code) 202-696-0284 22c. OFFICE SYMBOL ONR

FOREWORD

This report summarizes mostly experimental work conducted during the second year, October 1, 1989 to September 30, 1990, of DARPA/ONR Contract N00014-88-C-0714, High Temperature Ceramic Superconductors. Dr. Frank W. Patten is the DARPA program manager and Dr. Wallace Arden Smith, Materials Division, Department of the Navy, ONR, is the Navy project scientist.

Also included as part of this summary technical report is an appendix which covers more detailed experimental aspects of the work performed during the course of the research program.

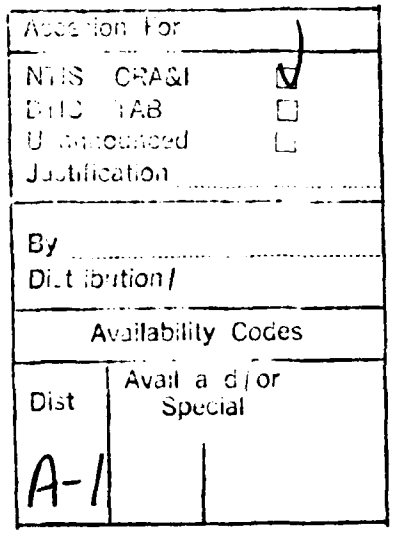

CONTENTS

1. INTRODUCTION AND BACKGROUND

1.1. MATERIALS DEVELOPMENT STATUS

High temperature ceramic superconductors (HTS) for various applications continue to be at the forefront of materials research and development since their dramatic discovery in 1986.

Much progress has been made during the past four years since the long-standing record critical temperature (T_c) of ~23 K for Nb_3Ge was exceeded. Some of the milestones were the report of $T_c \simeq 30$ K in the La-Ba-Cu-O system (Ref. 1), the discovery of the 1-2-3 class of perovskite ceramics with T_c as high as 94 K (Ref. 2), and the discovery of the $Bi_2Sr_2Ca_2Cu_3O_8$ ($T_c \sim 110$ K) (Ref. 3) and $TI_2Sr_2Ca_2Cu_3O_8$ ($T_c \sim 125$ K) systems (Ref. 4). The bismuth material is currently synthesized with 5 deg of its melting point. The thallium material is hazardous and toxic and must be handled with great care. The $YBa_2Cu_3O_7$ (designated 123) material is the most studied, and its chemistry is the best understood. As opposed to the thallium and bismuth materials, the (123) must be annealed in oxygen in the temperature range of 450° to 550°C, after its synthesis above 800°C.

Recent studies have revealed difficulties with the preparation of bulk high T_c ceramic superconduct materials. They are structurally complex and highly anisotropic. Stoichiometry is difficult to maintain. In addition, they require long high temperature anneals of heat treatment, when dense (which can cause reactions with container materials). Reproducibility and reliability are significant concerns, and the environmental stability of these materials remains uncertain. The status of bulk high temperature superconducting materials that are necessary for high power applications is not as advanced as in the case of electronic

devices that may be grown as epitaxial films. Quality samples of bulk HTS material, needed on a production scale to support a growing technology, do not exist at present. However, in spite of this, some very encouraging results are being obtained. Experimental short length samples, capable of sustaining current densities of 10^3 to 10^4 amperes/cm^2, have been reported. The transport critical current densities, J_c, of bulk superconductor, even in the absence of an applied magnetic field, are far below those achieved in single crystals or tin films (Refs. 5 and 6). The application of a magnetic field further reduces the J_c values in most materials too low to be of practical use in most applications. One explanation that has been put forward is that, in the bulk, the coupling across the grains is not as good as that in the film. This may be due to voids, secondary phases on the grain boundaries, and the nature of grain orientation. It is informative to note that whenever the J_c values of $\sim 10^4$ amperes/cm^2 were observed for bulk high T_c materials, the samples tested had the following common features: ultrahigh purity, fine grain size (1 μm or less), near theoretical density (95%), and preferred crystallographic orientation (Refs. 7 and 8). These perovskite type materials are invariably difficult to process and brittle in nature. Thus, the problem of configuration has r c yet been successfully addressed.

Work on the production of bulk conductor forms, such as wires, cables, and tapes is just beginning. However, this work is driven by the realization that usable magnets and solenoids made from high T_c materials will be of major technological and economic importance. Their impact will be far reaching in both military and civilian applications.

The overriding issue in bulk superconducting materials today is that of materials synthesis and processing. In general, the HTS materials are made in bulk form by a number of approaches. The simplest is, of course, milling together of binary oxides and/or carbonates. This method can be highly effective in making laboratory samples, but it lacks control of particle morphology and requires long milling times

to achieve homogeneity and small particle size. Chemical methods of preparation include coprecipitation methods (Refs. 9 and 11) and sol-gel (Refs. 9, 12, and 13) processes. While in principle these methods appear to be more advantageous than milling, in practice their full potential has yet to be realized. Precursor powders have also been successfully produced by dry roasting nitrate solutions. Freeze drying (Ref. 14) of the solution produces uniform fine powders. Related to these processes are the use of the aerosol flow reactor (Ref. 15) and the total combustion burner (Ref. 16), where aerosol droplets are formed from suitable inorganic salt solutions. Regardless of powder precursor source, the bulk forms are made only by high temperature processing, i.e., temperatures of 900° to 1000°C. This makes reactions with container materials difficult to control, and purity of the HTS is difficult to achieve. In addition to processing difficulties, the oxygen content is difficult to control, especially in dense bodies, and very temperature dependent, reproducible samples of good quality are difficult to ensure. Deposition processes which involve large kinetic energies at the deposition surface [laser ablation, plasma assisted chemical vapor deposition (PCVD), sputtering] can produce superconducting films without the high temperature anneal required by other routes, but they are limited in thickness to films around 1 μm and deposition on reasonably flat substrates.

The second critical issue is to understand processing/microstructure/properties relationships and the underlying physical properties, particularly J_c and flux pinning issues. This task will not be easy because in processing ceramic materials, in general, the goal is to obtain a uniform fine grained material in order to obtain the best mechanical properties. This is of particular importance in ceramic materials that exhibit large anisotropy in thermal expansion, where studies have shown that microcracking occurs when grain size in a randomly oriented structure exceeds a critical value determined by the material parameters (Ref. 17), as may be expected considering the large

anisotropy in the thermal expansion of yttrium barium cuprate, especially at the tetragonal to orthorhombic transition. The phase instability not only results in mechanical property degradation; but also the microcracks act to limit the electrical contact between grains, which contributes to the weak link behavior in the bulk superconducting properties of these materials. A recent study (Ref. 18) has found a critical grain size of the order of 1 micron for randomly oriented 123 compound. It is therefore apparent that in order to achieve high values of J_c in bulk material, dense material with grain size less than this must be produced. Due to the anisotropy in the superconducting properties of these materials, it is also necessary to produce grain-aligned material in order to obtain the maximum J_c. It may be expected that the production of aligned material will relax the grain size requirement somewhat, but if alignment is less than perfect, effects of anisotropy in thermal expansion will still be evident.

In view of these observations on processing, it is evident that beside grain boundaries, which are the dominant cause of low J_c in 123 polycrystalline material, a number of other factors may also contribute to decreasing the attainable critical current densities. The relative importance of issues such as grain-boundary phase, carbonate retention, environmental stability, mirco- and macrocracking phenomena, etc., remains to be addressed. Thus, it is clear that assessing the influence of any one factor requires careful control of the others and that attainment of the highest J_c may require simultaneous optimization of several of these factors.

1.2. MATERIALS RESEARCH PROGRESS, NEEDS, AND OPPORTUNITIES

1.2.1. Current Density Limits

Properties of HTS materials are steadily improving as processing techniques are gradually improved and the parameters influencing them are understood better. The thousands of researchers at hundreds of laboratories working on these problems represent a scientific investigatory

body with vast capabilities. Correspondingly, the current-carrying limits and magnetic field tolerance of HTS materials have been improved in the last year, and there is no reason to suspect that this process is slowing.

It is now understood that two fundamental hurdles must be overcome to produce HTS conductors that enable significant improvements in systems. These hurdles are (1) weak intergrain links and (2) weak flux pinning.

Intergrain links are the electrical contacts between individual grains of the HTS materials, and these contacts are generally resistive as a result of crystal misalignment and contamination at grain boundaries aggravated by the very short coherence lengths in these materials. Weak intergrain links result in low current limits and sensitivity to magnetic fields.

As the intergrain links are improved, wire will become feasible with moderate-to-good properties. In particular, it is likely that wire with about 10 kA/cm^2 at a field of 1 Tesla and a temperature of ~50 K should be achievable in unlimited lenghts (research materials are now approaching this performance).

Recently, considerable progress has been achieved regarding intergrain contacts. Bulk HTS material has displayed low-field current limits as high as 20 to 75 kA/cm^2 following liquid phase processing (U. Houston and AT&T Bell) or hot forging (Rockwell Science Center) of the "YBCO" material. The Houston and AT&T samples also retained up to 4 kA/cm^2 at fields of 1 Tesla. These results indicate that sufficiently strong intergrain contacts are possible, given the correct processing steps.

Once the weak intergrain link problem is resolved, flux pinning will be the major hurdle for improving bulk conductors. Flux pinning

is essential for high field applications and especially for ac or time-varying applications. The magnetic flux lines are pinned, or held in place, by microscopic regions of nonsuperconducting material. Arranging such pinning centers in the HTS material without destroying its overall superconductivity is a major challenge.

If strong flux pinning can be arranged, in addition to good grain-to-grain contacts, then wire with superior electromagnetic properties should result, exhibiting as much as 100 kA/cm^2 in fields of several Tesla at temperatures up to 77 K.

Three promising techniques for improved flux pinning have already been demonstrated. One involves neutron irradiation of the bulk material, creating isolated defects that pin flux lines and result in higher field tolerance within a grain. In a related development, proton beams were used to create nonsuperconducting regions deep within HTS grains, similarly resulting in flux pinning sites. The third approach uses excess copper in the formation in order to "precipitate" extra CuO planes at pinning sites. Even at the present early stage in the development of these approaches, the material properties available would be sufficient for many applications if they were incorporated in a practical wire or other conductor configuration.

1.3. PROGRAM OBJECTIVES

The principal goals of this program are (1) to demonstrate fabrication of high-temperature ceramic superconductors via a sol-gel method that can operate at or above 90 K with appropriate current density, J_c, in forms useful for application in resonant cavities, magnets, motors, sensors, computers, and other devices; and (2) to fabricate and demonstrate selected components made of these materials, including microwave cavities and magnetic shields.

The General Atomics (GA) approach is to develop the sol-gel technology processing of high-temperature ceramic superconductors to make sol-gel a viable process for fabricating high T_c (90 K) superconductors in forms useful for applications. The nature of sol-gel processing makes it inherently amenable to fabricating the thin films and fibers that are needed for many applications. In addition, the relatively low temperature characteristics of sol-gel processing make it advantageous for many applications in which the superconducting materials must be applied to heat sensitive substrates.

The scope of the effort includes the following:

- Synthesis of sol precursors.
- Optimization of sol-gel processed materials, including purity, homogeneity, stoichiometry, sintering temperatures, grain size and orientation, and dopants for grain boundary and flux pinning and for control of mechanical properties.
- Fabrication of forms, including powders, thin and thick films, and fibers.
- Evaluation of environmental stability, physical, mechanical, electrical, and magnetic properties.
- Fabrication and testing of a model component.

1.3.1. Project Outline

This program has been divided into six tasks: (1) metal alkoxide synthesis and processing, (2) microstructural evaluation and property measurement, (3) electrical and magnetic property measurement, (4) superconductor ceramic processing, (5) component fabrication and demonstration, and (6) reporting.

Task 1 is to synthesize a homogeneous metal alkoxide, $M(OR)_n$, where n is the valence of metal, M, and R is an organic group, solution that contains all the constituent elements which can be easily made to powders, thin film, or drawn into fiber form. Ideally, this solution should possess precise stoichiometry, adequate stability, polymerizability, adherence, and spinnability. Also, the polymeric materials formed from this solution should be thermosetting, be able to be dissolved in organic solvents, and contain as little as possible low-temperature pyrolyzable organics with high char yield.

Task 2 is to study the microstructure as a function of processing parameters. The study includes: density, pore size and pore size distribution, phase identification, chemical composition and purity, environmental stability, effects of heat treatment, residual strain, seeding, annealing in magnetic fields, and epitaxy on grain growth and orientation.

Task 3 is to study the electrical and magnetic properties of the $YBa_2Cu_3O_{7-x}$ (123) high T_c ceramic superconductors. It will include both the ac electrical resistance (R_{ac}) and the ac magnetic susceptibility (χ_{ac}) magnetic properties.

The dc current versus voltage curve will be measured at liquid nitrogen temperatures for all promising superconducting materials and a value for J_c (77 K) determined. For the samples with the highest values of J_c (77 K), critical currents will be measured as a function of magnetic fields of up to 8 Tesla at temperatures between 1.4 K and near the superconducting transition temperature T_c. These data will be collected in liquid He or flowing He using a Janis Supervaritemp dewar equipped with an 8 Tesla superconducting magnet. As required, Hall effect measurements can be performed in this apparatus to determine the type and density of the current carriers. Both χ_{ac} and R_{ac} at pressures up to 20 kbar, can be used in this dewar to measure the superconducting and

magnetic properties of samples at high pressures, at high magnetic fields, and at temperatures from 1.4 to 300 K.

As a subcontractor to GA, the Superconductivity and Magnetism group, under the direction of Professor M. Brian Maple, at the University of California, San Diego (UCSD), has performed the electromagnetic characterization of high-temperature superconducting oxide compounds, which are fabricated at GA. UCSD personnel have and will continue to measure the superconducting and magnetic properties by means of measurements of the upper critical magnetic field, critical current density inferred from both direct and magnetization measurements, magnetic susceptibility, Meissner effect, and specific heat.

Task 4 is an investigation of superconductor ceramic processing. Most of the important applications of superconductors require material in the form of fiber or films. Magnets, conductors, motors, and generators are examples of applications employing fiber; while detectors, microwave cavities, and microcircuitry require superconducting material in the form of films. The sol-gel process is ideally suited to producing materials in these forms; in fact, it is used commercially to produce antireflection and mirror coatings and to produce continuous ceramic fibers for structural reinforcement in composite materials and for thermal insulation.

Originally task 5 was to demonstrate component fabrication. GA under the original SWO had to design and build a high Q, high T_c superconducting cavity using its unique sol-gel coating process capabilities. This task would have proceeded after some initial coating tests verified dc superconductivity and questions of adhesiveness, surface preparation, and processing procedures are answered. As the fabrication process and the materials quality were improved throughout the three-year program, two additional cavities would have been constructed and tested. Coupling would have been through a waveguide inductive iris into an end wall with a logarithmic decrement technique of Q measurement were

considered most appropriate for the high Q anticipated. An X-band (10 GHz) frequency choice allows for convenient dimensions of 4.3 cm diameter by 2.8 cm height. However, DARPA/ONR recent recommendation to GA was to curtail the work on the cavity and concentrate on improving the quality and transport properties of solution condensed films activity.

2. SUMMARY OF ACCOMPLISHMENTS

In the following section, a brief narrative description of the major advances that have been accomplished under the subject contract are presented.

2.1. SOL-GEL PRECURSORS

1. Prepared stable homogeneous 123 precursor solution.
2. Achieved precise 123 stoichiometry for phase purity.
3. Polymerized solution to high char yield thermosetting resin.

2.2. FIBER SPINNING AND EXTRUSION

1. Optimized viscosity and solution rheology, defined phase relationships.
2. Spun continuous 50 to 200 μm diameter 123 preceramic fibers.
3. Achieved necessary green strength and coherence.
4. Developed process for low shrinkage extruded material.

2.3. FIBER CURE AND PYROLYSIS

1. Obtained complete organic removal without stable $BaCO_3$ formation.
2. Obtained refine grain size in spun fibers.
3. Reproducibly obtained 1500 to 2000 A/cm^2 at 77 K in spun fibers.
4. Obtained up to 1000 A/cm^2 at 77 K in extruded rods.

2.4. THIN FILMS

1. Dip coated 123 films on metal and ceramic substrates.
2. Obtained significant grain alignment on Ag substrate.
3. Ag disk and cylinder were coated.

2.5. FLUX DYNAMICS

Demonstrated that Pr doping improve flux pinning.

3. PUBLICATIONS AND PRESENTATIONS

3.1. PUBLICATIONS

1. Chen, K. C., and K. S. Mazdiyasni, "High T_c Superconductor Fibers from Metallo-Organic Precursors," MRS Proceeding, 1990.

2. Chen, K. C., A. Y. Chen, and K. S. Mazdiyasni, "Metallo-Organics Derived Tractable Resins for YBCO Superconducting Fiber Fabrication," to be published in MRS Proceeding Better Ceramics Through Chemistry IV, 1990.

3. Stephens, R. B., "Flux Bundle Interactions," accepted for publication in Jour. of Mat. Res. Society, 1990.

3.2. PRESENTATIONS

1. Sung, S. P., and K. S. Mazdiyasni, "Sol-Gel Synthesis and Characterizations of Submicron High T_c Ceramic Superconducting Powders," Third International Conference on Ceramic Powder Processing Science, San Diego, California, February 4-7, 1990.

2. Chen, K. C., A. Y. Chen, and K. S. Mazdiyasni, "Sol-Gel Derived Soluable Resin for Y-Ba-Cu-O Superconducting Fiber Fabrication" presented at Materials Research Society 1990 Spring Meeting, Symposium A: Better Ceramics Through Chemistry IV, San Francisco, California, April 16-21, 1990.

3. Chen, K. C., A. Y. Chen, and K. S. Mazdiyasni, "Synthesis and Characterization of Tractable Resin for YBCO Superconducting Fibers Fabrication," presented at the 92th Annual Meeting of American Ceramic Society, Dallas, Texas, April 24, 1990.

4. Stephens, R. B., "Flux Bundle Interactions," presented at MRS Spring Meeting, Anaheim, California, 1990.

3.3. PATENTS

1. Chen, K. C., and K. S. Mazdiyasni, "Method for Preparing Rare Earth-Barium-Cuprate Preceramic Resins and Superconductive Materials Prepared Therefrom," U.S. Patent Application No. 441,955, pending.

2. Chen, K. C., and K. S. Mazdiyasni, "Method for In-Situ Prevention of Stable Barium Carbonate Formation in High T_c Ceramic Superconductors."

3. Montgomery, F., and K. S. Mazdiyasni, "Method for Preparation of Solution Condensed Phase Superconductor BYCO Thin Films."

APPENDIX A
THIN FILM AND FIBER PROCESSING

A.1. PRECURSOR MATERIALS

Two types of metal organics were used to develop 123 films on different substrates.

Homogeneous solutions have been prepared using $Y(OR)_3$, $Ba(OR)_2$, and the copper (II) mixed-ligand species $(C_3H_7O_2)_2Cu_2(u\text{-}OR)_2$, where R = $CH_2CH_2OCH_2CH_2OCH_2CH_3$ and $C_5H_7O_2$ = 2,4-pentanedionate (Ref. 19).

A.1.1. Experimental Procedures

The starting alkoxides, and the mixed-ligand copper (II) compound were prepared using the procedure described in a previous progress reports under this effort.

A.1.1.1. Preparation of 123 Precursor Solution. In order to determine the stoichiometry and processing effects on the electrical properties of superconducting films, four precursor solutions (Table A-1) were prepared following the procedure described in the quarterly progress reports (Ref. 20). The Y:Ba:Cu stoichiometry was varied in three of the solutions. The fourth solution was treated with hydrogen peroxide during the hydrolysis step.

A.1.1.2. Dip Coating. Dip coating was accomplished using the GA bench top dip coater. Usng the process flow diagram for the Cu(II) mixed-ligand is shown in Fig. A-1.

A.1.1.3. Electrical Property Measurements. Resistance measurements were conducted at UCSD using a Linear Research LR-400 Four Wire ac

TABLE A-1
STOICHIOMETRY OF HOMOGENEOUS SOLUTIONS
USED TO DIP COAT SUBSTRATES

	Stoichiometry Molar Ratio			Hydrolysis Conditions	
Solution	Y	Ba	Cu	H_2O	H_2O_2
10208-55	1.000	2.000	3.000	1.000	--
10208-83	1.028	2.000	2.998	1.003	--
10208-79	1.029	2.000	3.167	1.652	--
10208-97	1.028	2.000	2.994	1.003	0.198

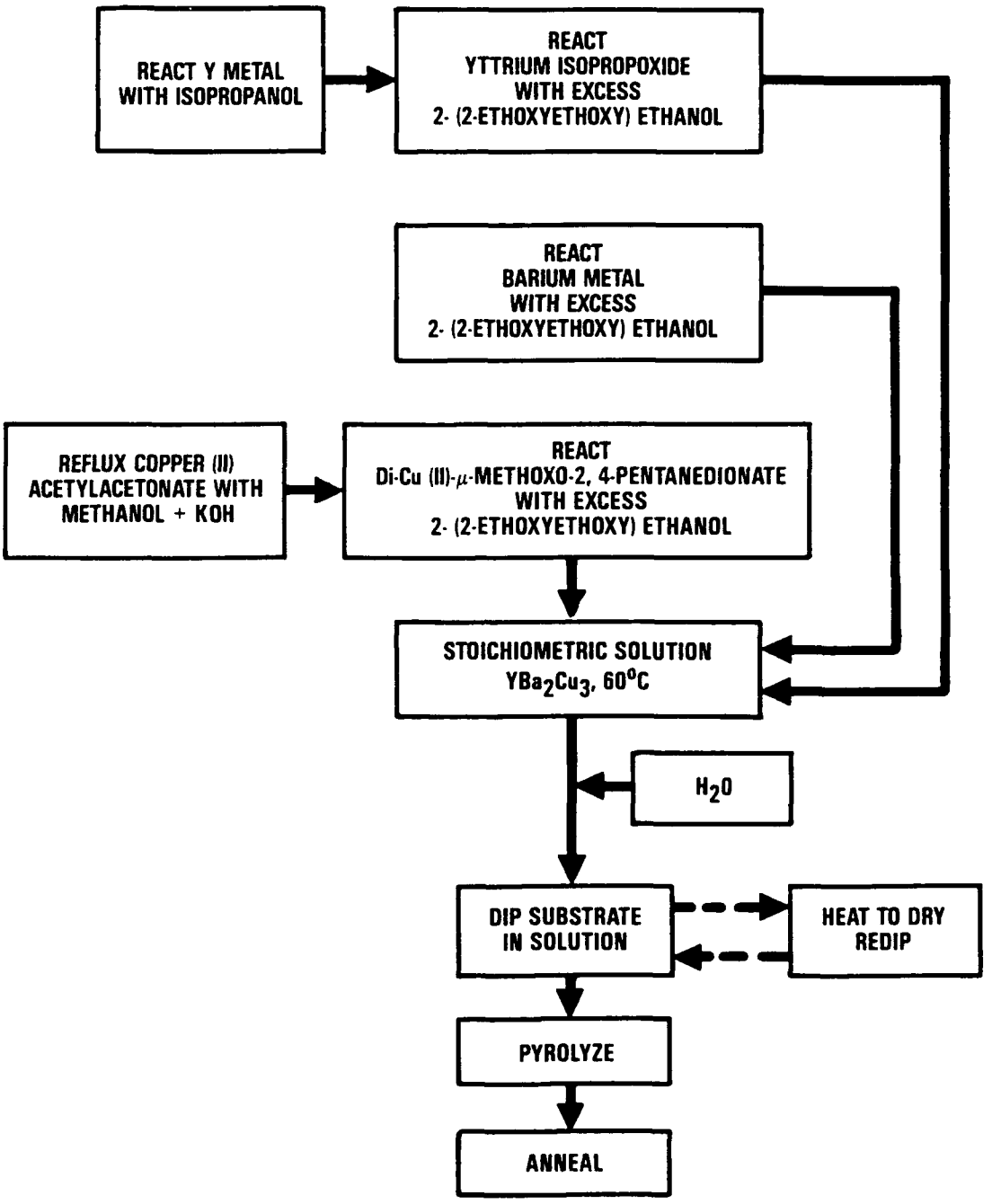

Fig. A-1. Process flow for Cu(II) mixed-ligand method

Resistance Bridge, with a current of 0.1 uA at 13 Hz. Silver wire leads were cemented to the 123 film with silver paste after sputtering 1 x 3 mm silver pads on the coating. The pads were positioned by preparing an aluminum foil mask which surrounded the sample piece. The current pads were spaced 1 mm from the voltage pads, and the voltage pads were 4 mm apart. Thus, about 12 mm^2 of the film was tested.

Durng this period, we have been investigating the effect that processing parameters have on the superconducting resistive transition. Figure A-2 shows the general characteristics of the transition from the normal state to the superconducting state for films prepared on yttria-stabilized zirconia polycrystals (YSZP). The electrical resistance of the films decrease as the sample is cooled from room temperature. Near the transition temperature, the resistance drops rapidly and approaches zero within a range of a few degrees K. However, the minimum resistance of the films, with voltage leads spaced 4 mm apart, was only 0.07 ohm.

In order to compare the effects of processing conditions on the transition, three parameters describing the transition can be defined. These parameters (T_{90}, T_{50}, T_{10}) are the temperatures (K) at which the Resistance is 90%, 50%, and 10% of the value extrapolated from decreasing resistance in the normal state. The width of the transition is, then, T_{90} and T_{10}. Furthermore, a symmetric transition would have the same number of degrees between T_{90} and T_{50} as there are between T_{50} and T_{10}. Table A-2 summarizes the processing conditions and the transition parameaters for several films made using the solutions in Table A-1. In addition, the normal state resistance at 100 K is also given in Table A-2.

The first two results in Table A-2 show that the thickness of the film affects the transition. Based on the weight of material deposited, the thickness of the film produced by four dips is 1 to 2 μm. Thus, the film dipped once would be 0.25 to 0.5 μm thick. The thicker film results in a sharper transition from the normal to the superconducting

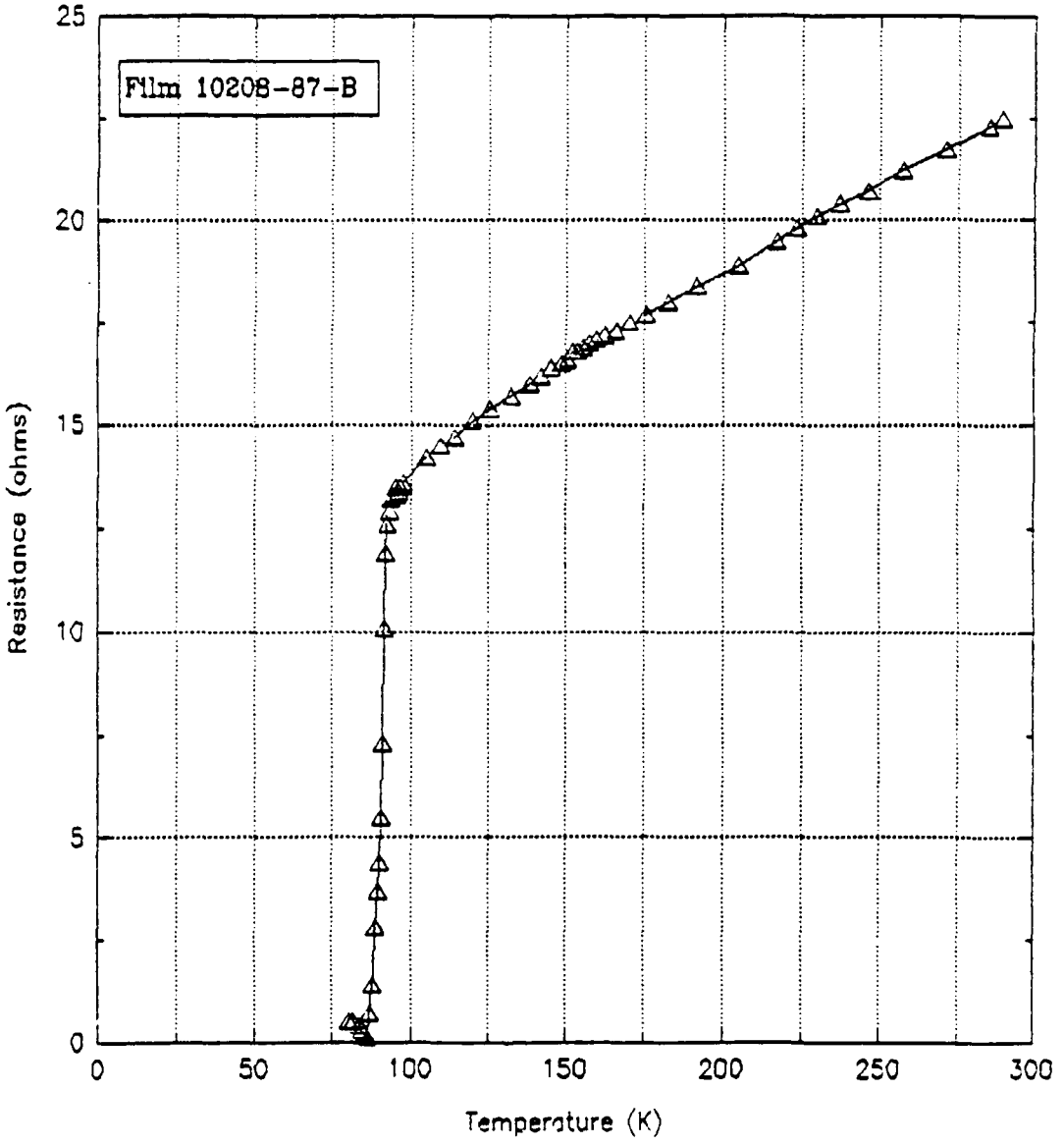

Fig. A-2. Resistance as a function of temperature for an $YBaCO_{(7-x)}$ film on YSZP

TABLE A-2
EFFECT OF PROCESSING PARAMEATERS ON THE
SUPERCONDUCTING TRANSITION PARAMETERS

Coating ID	Solution ID	Dip	Process	R100 ohms	T90 (K)	T50 (K)	T10 (K)
10208-105C	10208-83	4	t_{max} = 902[a] t_{min} = 406	15.8	93	91	87
10208-105E	10208-83	1	t_{max} = 902[a] t_{min} = 406	41.9	92	89	78
10208-72C	10208-55	4	t_{max} = 905[a] t_{min} = 404	17.1	92	90	85
10208-87C	10208-79	4	t_{max} = 905[a] t_{min} = 404	21.2	92	90	84
10208-87B	10208-83	4	t_{max} = 905[a] t_{min} = 404	14.6	92	91	87
10208-90B	10208-83	4	t_{max} = 911[a] t_{min} = 402	24.7	92	91	86
10208-90D	10208-79	4	t_{max} = 911[a] t_{min} = 402	8.3	92	91	88
10208-105B	10208-83	4	t_{max} = 921[a] t_{min} = 405	16.3	92.5	91	88
10208-116D	10208-83	4	(b)	9.9	93.8	90.8	87.3
10208-105A	10208-97	4	t_{max} = 921[b] t_{min} = 405	9.5	93.2	91.4	89.1
10208-117B	10208-97	4	(b)	8.3	92.9	90.6	86
10204-18A	10208-97	4	(c)	25.5	92.5	91.5	85

[a] 1°C/min to t_{max}; hold 10 min; 5°C/min to t_{min} hold 24 h.

[b] 5°C/min to 70; 1°C/min to 902; hold 10 min; 5°C/min to 500; 1°C/min to 403, hold 60 min.

[c] 1°C/min to 800; 0.5°C/min to 905; hold 10 min; 5°C/min to 404; hole 12 h.

state, and significantly lowers the initial resistance of the normal state. Currently, we feel that this is being caused by reaction of a certain volume of the film with the substrate.

In investigations of thin film deposition by various techniques, the detrimental effects of superconductor-substrate interactions have been reported (Ref. 21). The reaction of 123 (Y:Ba:Cu) with ZrO_2 is known to occur at temperatures as low as 600°C and at 945°C results in the formation of CuO, $BaZrO_3$ and the 211 compound (Ref. 22).

A preliminary observation indicating that reaction with the YSZP substrate may be occurring during the processing of sol-gel derived films from solution 10208-55 is given in Fig. A-3. The transition in this film began at 93 K and had a T_{90} and T_{10} width of 16 K. The scanning electron microscopy (SEM) photomicrograph shows the morphology of the film which had been processed following the (a) procedure in the footnotes to Table A-2 with t_{max} = 921°C. After a short etch with dilute HCl in methanol, two distinct layers are evident in the thick portion of the film at the bottom of the substrate. EDAX analysis of top layer (Y:Ba:Cu = 1.26:2.07:3.00) agreed with microprobe analysis (1.24:2.11:3.00) of specific areas on the surface of a film made from the same precursor solution 910208-55). The lower layer seems to be enriched in copper although broadening of the electron beam could have distorted the measurement of the compositional difference.

Also, the stoichiometry of the solution affects the sharpness of the superconducting transition of the film. The superconducting transitions for films prepared from the solutions in Table A-1 have a T_{90} of about 92 K. However, the magnitude of the foot on the transition is different for each solution. Microprobe analysis of the surface of the films indicates that the surface is not single phase 123. Instead, the films have areas with the correct stoichiometry interspersed with a phase that has the proper Ba:Cu ratio but is high in yttrium. In

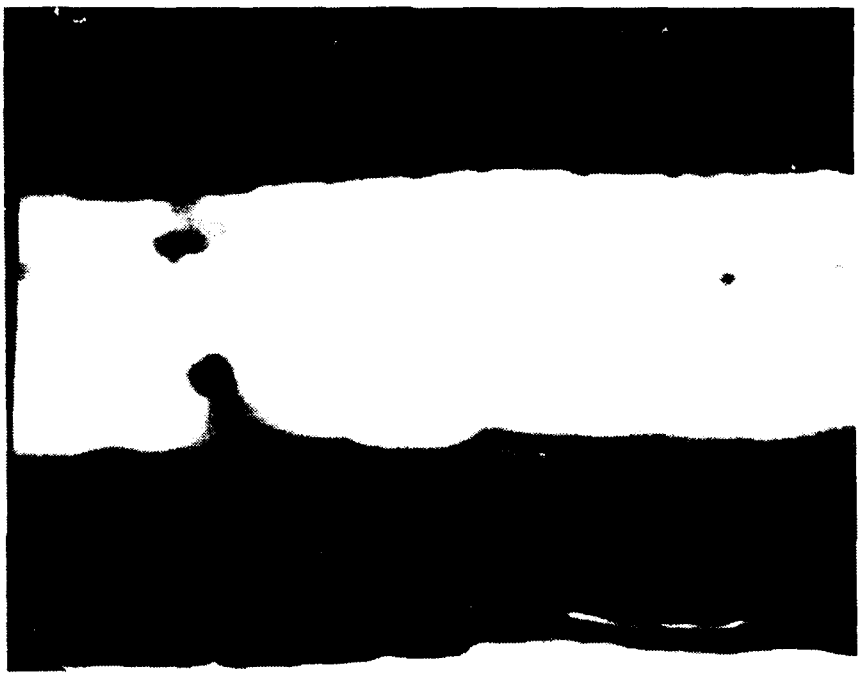

Fig. A-3. SEM photomicrograph showing morphology of superconducting film and apparent reaction layer

addition, there are some spots that are high in yttrium and depleted in copper. We are currently trying to eliminate these segregated areas.

Increasing the processing temperature does not have a large effect on the resistance of the film. The width of the transitions for films prepared from solution 10208-83 which were heated to 905, 911, and 921°C (±2°C) were similar. However, the resistance of the normal state at 100 K was higher for the 911°C processed film. The cause of variability of the high resistance of these films are not known at this time and are being investigated by analytical electron microscopy work in an attempt to understand and correlate the microstructure processing properties relationships.

Earlier in this program we found the H_2O_2 added to the hydrolysis solution resulted in a 123 powder that did not contain any low melting (<980°C) phase. Thus, solution 1028-97 was prepared using H_2O_2 during hydrolysis. The electrical properties of the films prepared from this solution were similar to those prepared without the additive.

Several entries in Table A-1 show the resistance transition of films from the same solution processed in three different ways. The samples that were cooled slowly between 500° and 403°C with only a 1 h hold had the same properties as did the samples oxygenated for a longer time. Thus a 24-h oxygenation may not be required to obtain a sharp resistance drop at 92 K.

The rate at which the sample is heated to about 800°C does appear to affect the magnitude of the 100 K resistance. The resistance of the film that was heated at 0.5°C/min was about three times higher than a similar film heated twice as rapidly to the same maximum temperature.

A.1.1.4. 123 Film on $SrTiO_3$. Thin films of Y123 were prepared by dipping single crystal $SrTiO_3$ in a sol of the 123 resin in toluene and i-PrOH shown in flow diagram A-4, which currently has been used to make

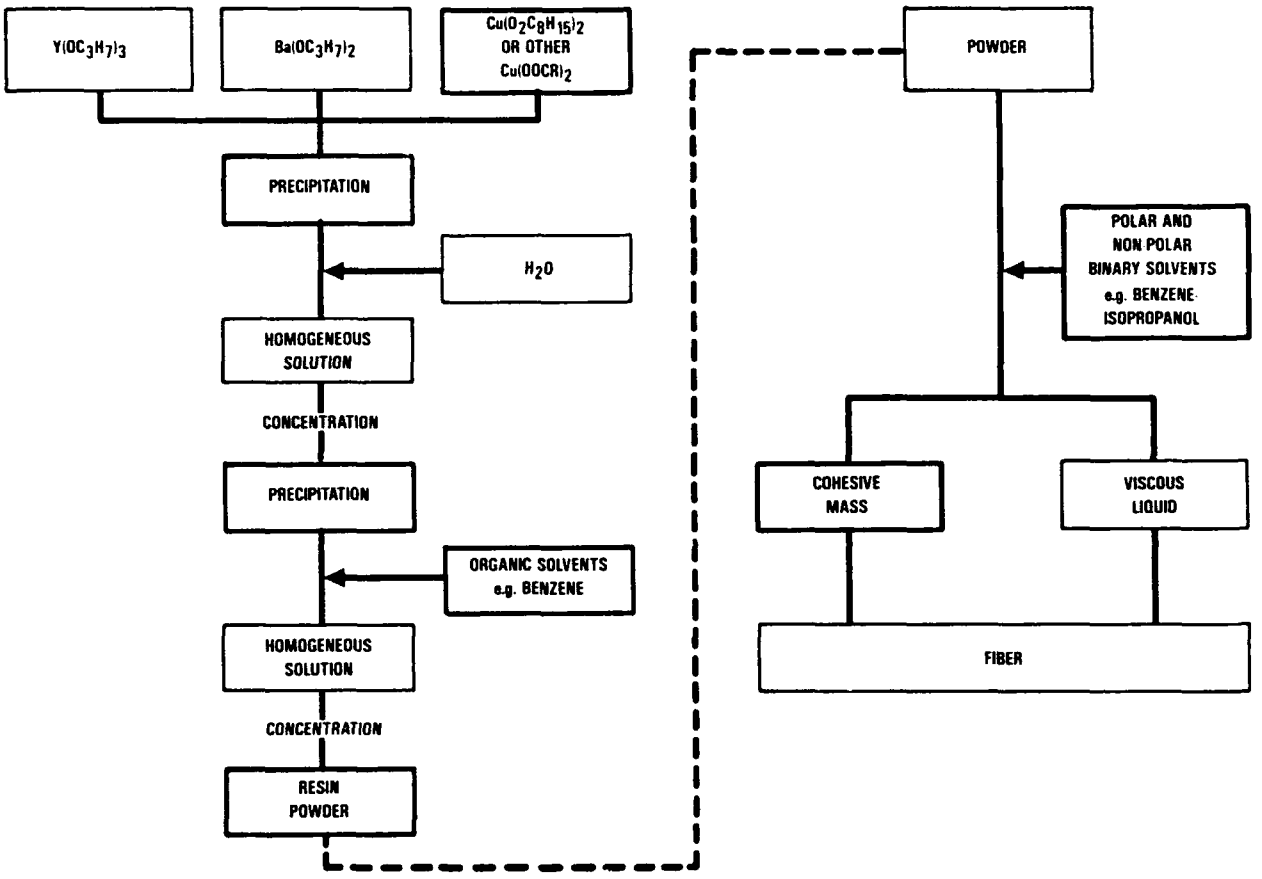

J-033(7)(a)
10-16-90

Fig. A-4. Process flow for Cu(II) 2-ethylhexanoate method

123 fibers. The concentration of the resin was approximately 30 w/o and the ratio of toluene to i-PrOH was 4:1. The substrate was multiply dipped in air and pyrolyzed at 500°C in between each dip. Thus obtained film was fired at 825°C for 1 min in flowing O_2. The purpose of low temperature and short time firing was to minimize the chemical reaction between the substrate and the film. The film was fully oxygenated by holding at 400°C for 19 h in flowing O_2 atmosphere.

As the resistance curve (Fig. A-5) shows, the film exhibited a metallic characteristic. The measured T_c was approximately 80 K and J_c =400 A/cm^2 at 30 K at 0 field. The XRD pattern (Fig. A-6) shows the film is highly oriented with its c-axis perpendicular to the substrate surface. The J_c value is anticipated to be much higher than observed because the film thickness was not measured accurately. The J_c calculation was made by overestimation, using an arbitrary film thickness of 1 μm. It is expected that the J_c is to improve drastically with further work on processing optimization. For example, the SEM photograph (Fig. A-6) shows the film is still quite porous and not fully crystalline.

A.1.2. 123 Film on Silver (Ag)

With superconductivity well demonstrated using the present system on $SrTiO_3$, the next task was to demonstrate the same on more practical substrates such as polycrystalline Ag and YSZP. Since it is crucial to develop a highly dense and smooth film for most applications, it was necessary to determine the right heat treatment schedule for full densification and the attainment of fine grain size. Because of its inertness and thereby the absence of complications in analysis, Ag was chosen as the substrate material for this study.

Figure A-8 shows the film morphologies observed after heat treating to various temperatures and times. The SEM photographs show that full densification does not occur even at 920°C for 10 min. However, by holding at 920°C for 3 h, full densification was achieved. It is worth

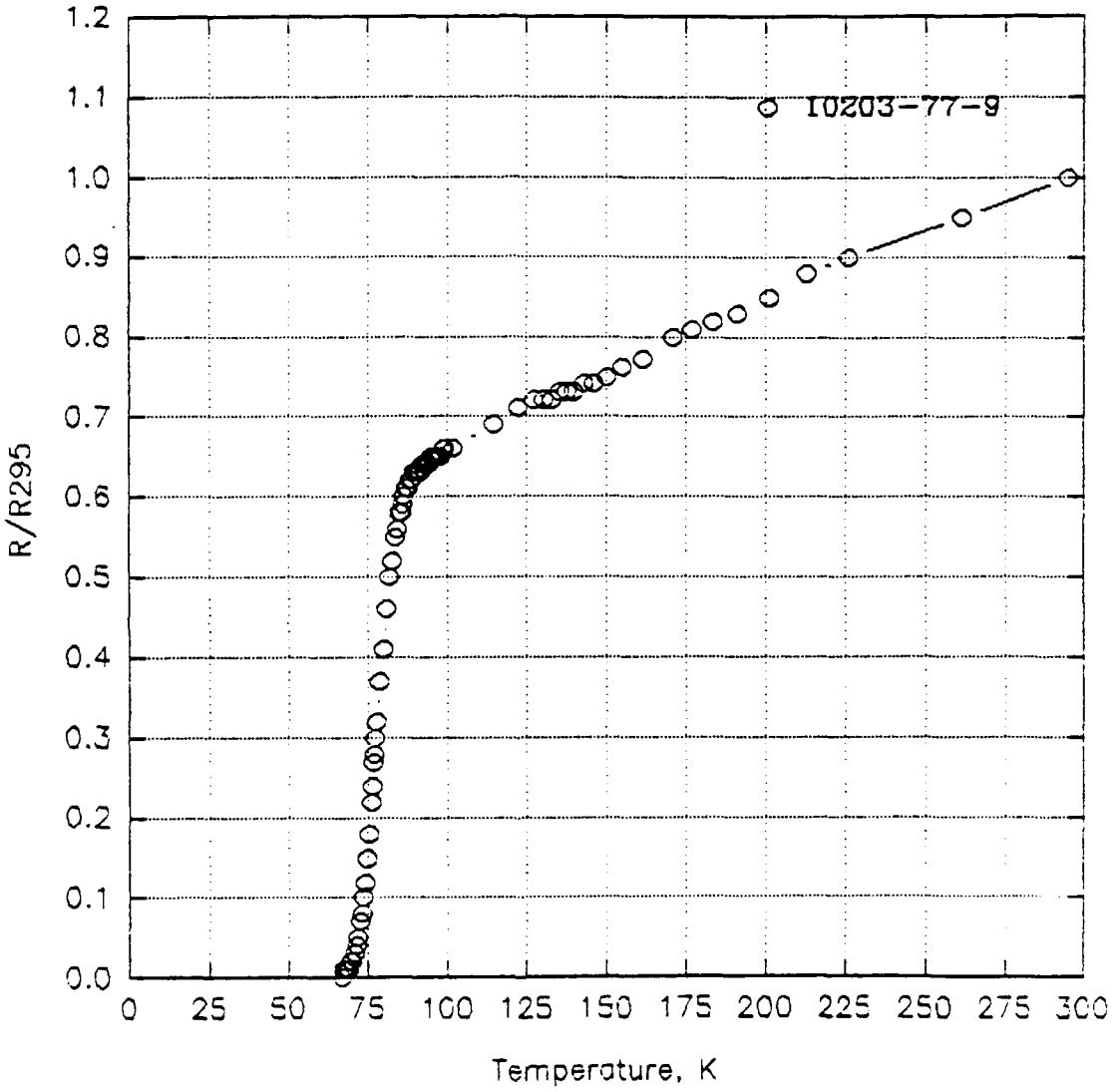

Fig. A-5. Resistance versus temperature curve for the 123 film on $SrTiO_3$

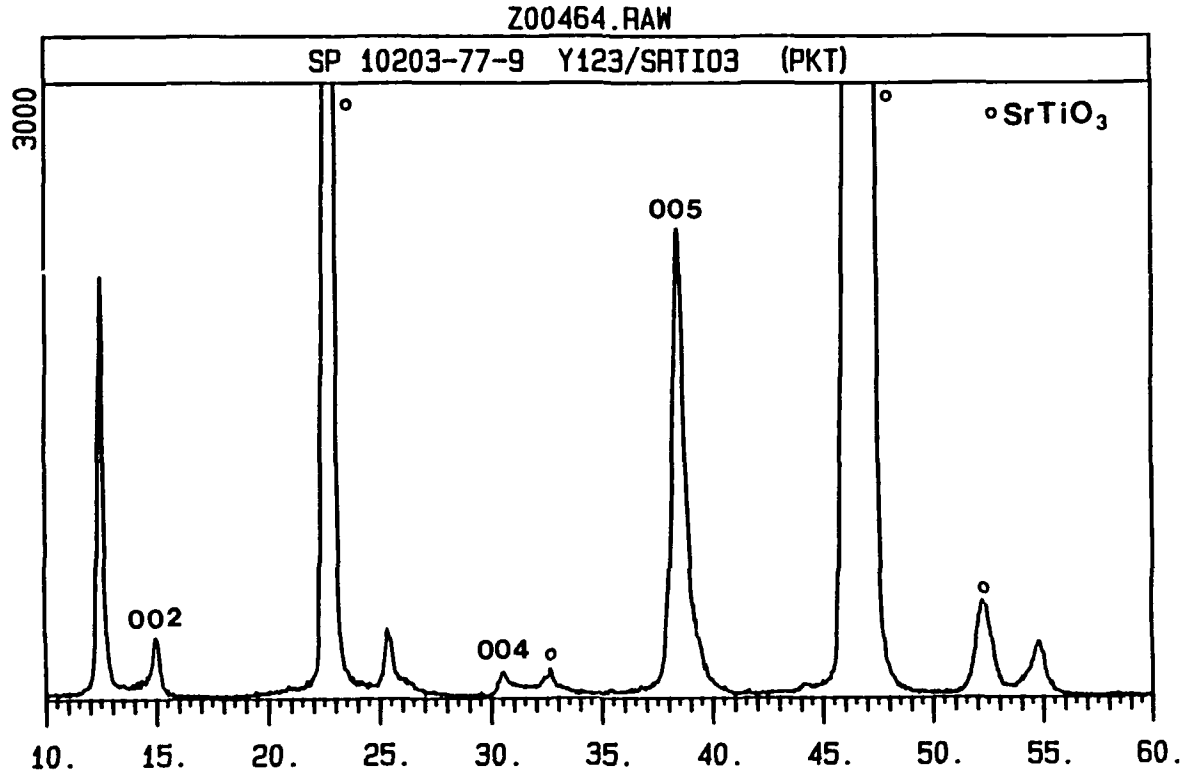

Fig. A-6. XRD pattern of 123 on $SrTiO_3$

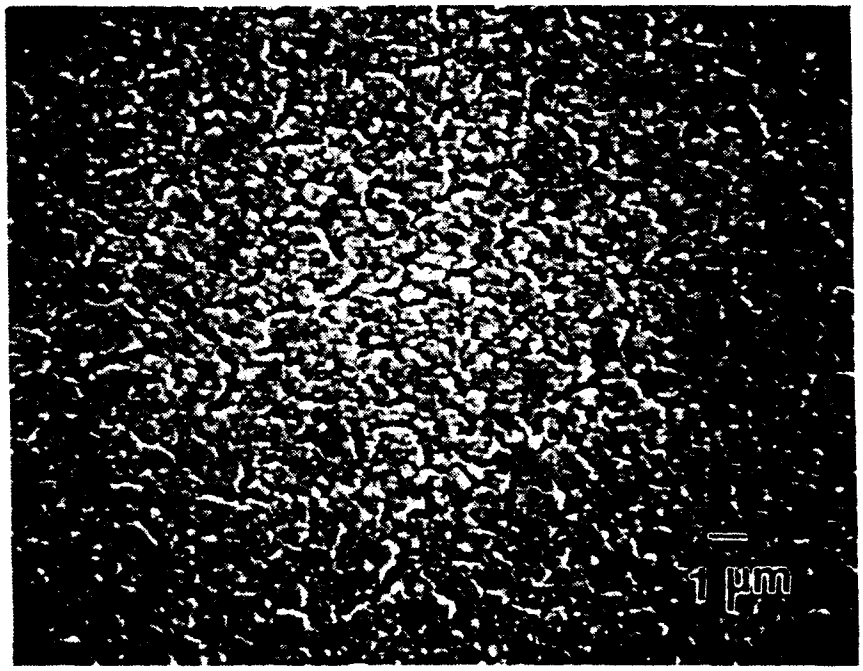

Fig. A-7. SEM photograph of 123 on $SrTiO_3$

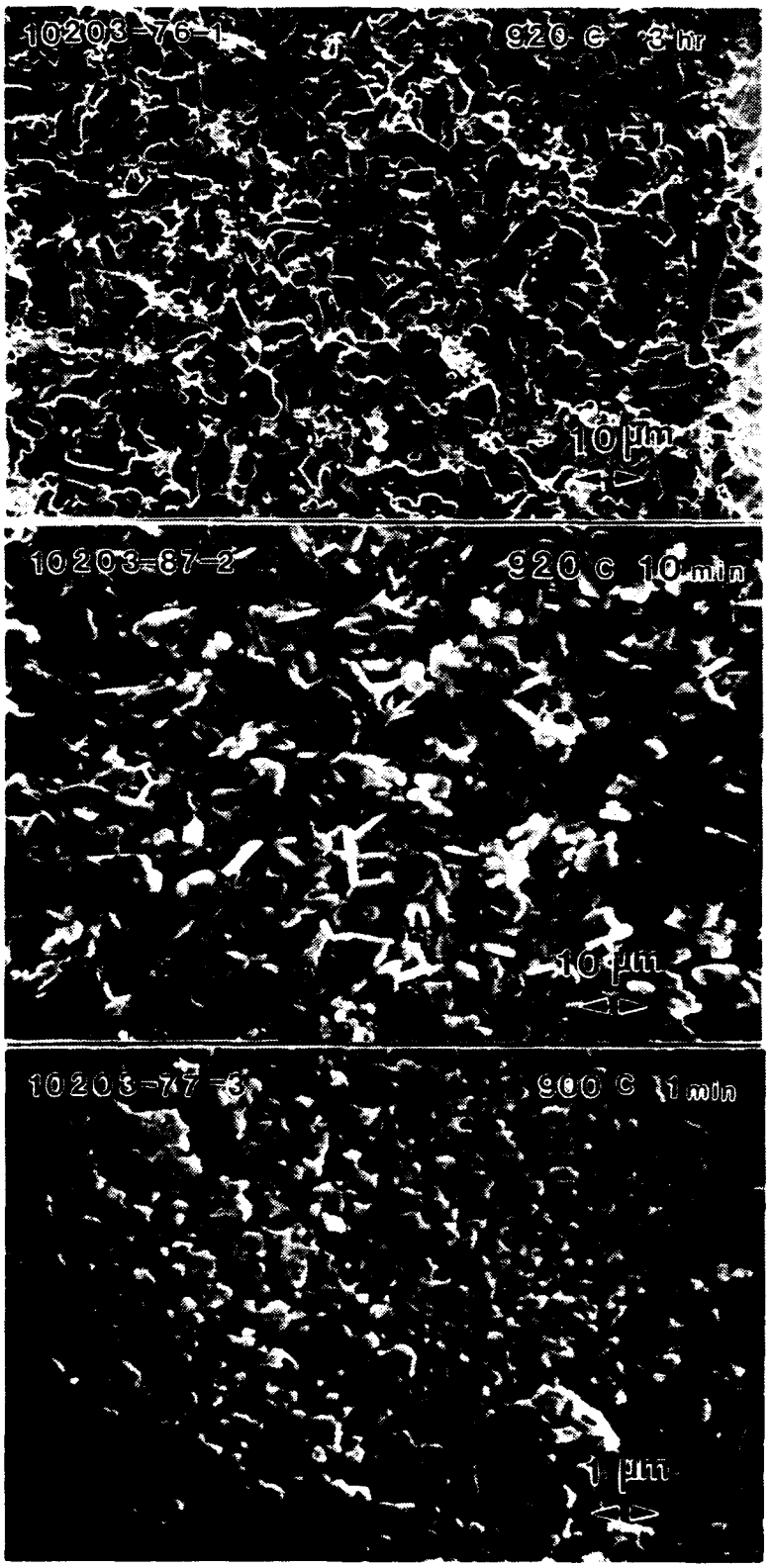

Fig. A-8. SEM photographs of 123 film heat treated at the indicated temperatures and times

noting, however, that numerous microcracks occurred as a consequence of thermal expansion mismatch. It has been shown that finer grain size would minimize or eliminate the microcracking and that a heat treatment at 920°C for approximately 30 min will remedy the situation.

A.1.2.1. Grain Alignment. During the study to determine the right heat treatment condition, it was observed that a high degree of c-axis orientation was attained at elevated temperatures. As shown by the XRD patterns in Fig. A-8, (001) peaks are enhanced when the films were heat treated beyond 920°C for 10 min. As observed in the SEM micrographs (Fig. A-8), the degree of alignment improved with increasing isothermal holding time. For example, the ratio of (006) to (110) peaks was 12 for the sample heat treated for 30 min at 920°C, where as it was 200 for the sample held at the same temperature for 3 h.

Since it was difficult to measure the quality of the film on Ag by dc resistance, due to the exceptionally low resistivity of silver, dc susceptibility measurements were carried out at UCSD and the results are shown under electromagnetic property characterization.

A.1.2.2. Ag Substrate Effect on Alignment. In order to test whether grain growth of Ag was responsible for c-axis alignment, a pair of Ag substrates were prepared. One was heat treated in O_2 at 920° for 10 min and the other was left untreated. The heat treatment caused the Ag grains to grow to a size approximately 1 mm in diameter. The two substrates were dipped simultaneously and heat treated at 920°C for 30 min in flowing O_2.

The XRD results (Fig. A-9) show the film on heat treated Ag was aligned twice as much as the one without the heat treatment. This suggests heteroepitaxial growth and needs further investigation for confirmation.

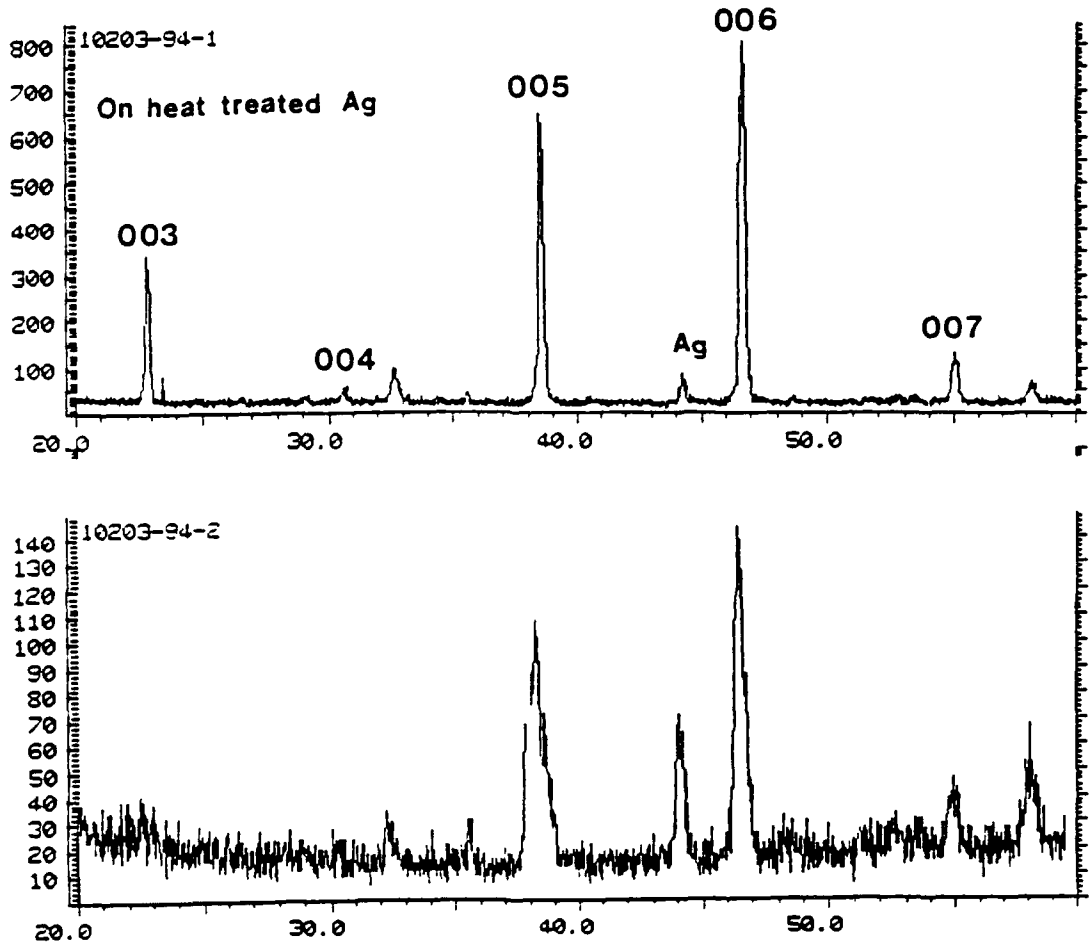

Fig. A-9. XRD patterns of the 123 films prepared on heat treated (upper figure) and untreated (lower figure) Ag substrates

A.1.2.3. 123 Film on YSZP. As stated previously, 123 is known to react with YSZ at temperatures beyond 900°C. This fact, combined with the information we have gained from the Ag work, that is a heat treatment at 920°C for greater than 10 min is necessary for full densification, it became apparent that a minimum 123 layer thickness is required to compensate for the inherent reaction that occurs with YSZP substrate.

For this study polished YSZP substrates were dipped 9, 12, and 20 times in air, pyrolyzed at 500°C and heat treated at 920°C for 10 min in O_2. Figure (A-10) shows the standard 4 point probe resistance curves obtained from the study. It is clear that with increasing thickness, the transition width sharpened dramatically. It appears that the film needs to be dipped at least 20 times, which corresponds to approximately 2 μm in thickness.

Since 20 dips are extremely time consuming and more importantly, often linked with surface irregularities, a feature intolerable in a high Q cavity, a new solvent was employed. By using normal hexane, C_6H_{12}, instead of toluene, the resin could be concentrated to as high as 50 w/o without causing precipitation. As a reminder, the highest solid concentration the toluene system would allow, without causing precipitation, was approximately 30 w/o. With the new sol, only five to six dips were required to build up the same coating thickness.

A.1.3. Preliminary 123 Coated Complex Shapes

Since promising results were obtained on Ag, a silver cylinder and a disc were machined, cleaned, and coated with a freshly prepared sol. They were subsequently fired at 920°C for 30 min and annealed at 500°C for 12 h. Figure A-11 shows that smooth coatings were obtained and their superconducting properties measurements are in progress.

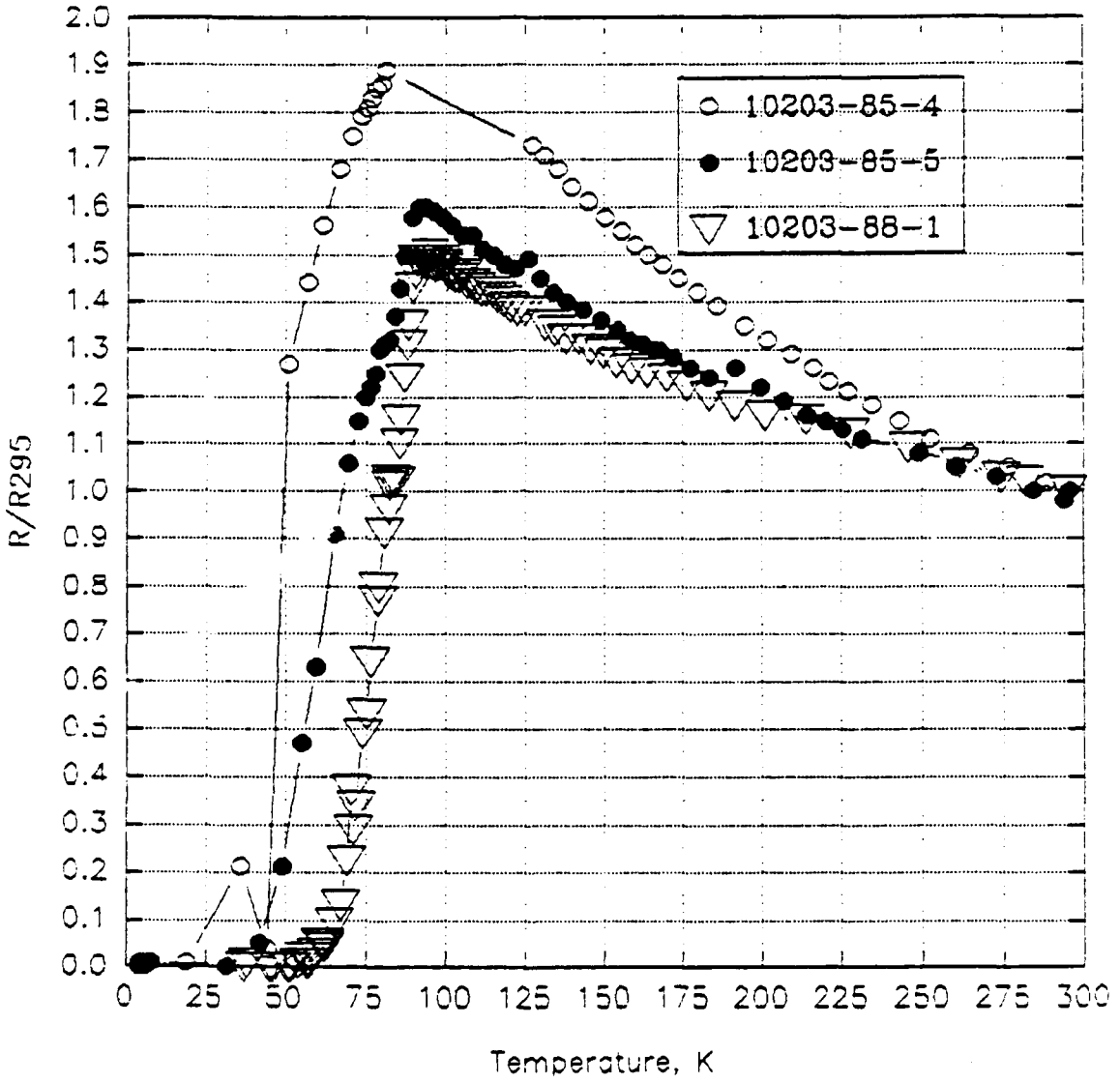

Fig. A-10. Resistance versus temperature curves for 123 films on YSZP. The open circles represent 9 dips, closed circles 12 dips, and inverted triangles 20 dips.

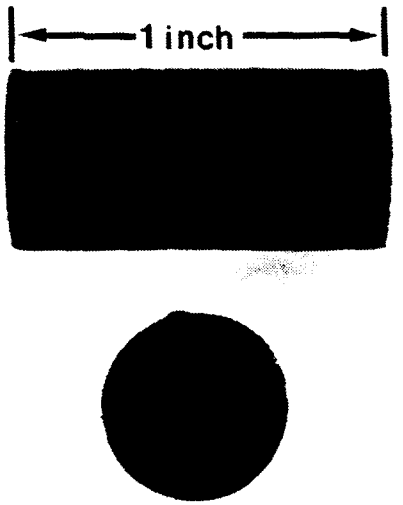

A

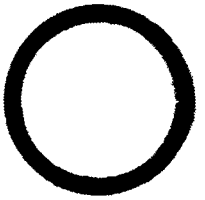

B

Fig. A-11. 123 coatings on an Ag cylinder and a disc. The bottom photograph is the top view of the cylinder

A.1.4. Thick Films

Since detailed microstructural analysis of the 123 film on any given substrate was found to be difficult to attain, a thick film of 123 was made by placing a drop of highly concentrated 123 precursor on Teflon substrate and oven dried to ~300°C and processed in an identical manner than a thin film. The thick film prepared by this technique, although cracked, provided large free standing 123 superconducting pieces which could be characterized by DTA, TEM, and electromagnetic property measurement as function of temperature. The DTA indicates highly phase pure 123 as shown in Fig. A-12. The TEM of the ion milled sample indicate very dense and twinned material with no evidence of impurities around the grain boundaries (Fig. A-13). However, there were evidence of some nonsuperconducting tetragonal phase shown in Fig. A-14 within the orthorohmbic grain which could account for low J_c observed in these materials. Also there are preponderance of cross twinning of the grain throughout the microstructure as shown in Fig. A-15. The resistance curve is extremely sharp with onset of superconductivity at 92.5 K and zero resistance was reached at ~91 K (Fig. A-16).

A.2. FIBER PROCESSING

A.2.1. Extrusion of 123 Filaments/Rods

Since the fibers hand-drawn or spun from all sol-gel preceramic resin undergoes a large shrinkage, 50% or more, during organic pyrolysis and sintering which often results in cracking and weak fibers; 123 powders were used as filler material with the preceramic resin to reduce the shrinkage during firing.

Two kinds of 123 powder were utilized: one commercially available powder from Rhone-Poulenc and another experimental laboratory powder from the Argonne National Laboratory. The DTA and XRD have been performed to characterize the as-received and after-calcined 123 powders.

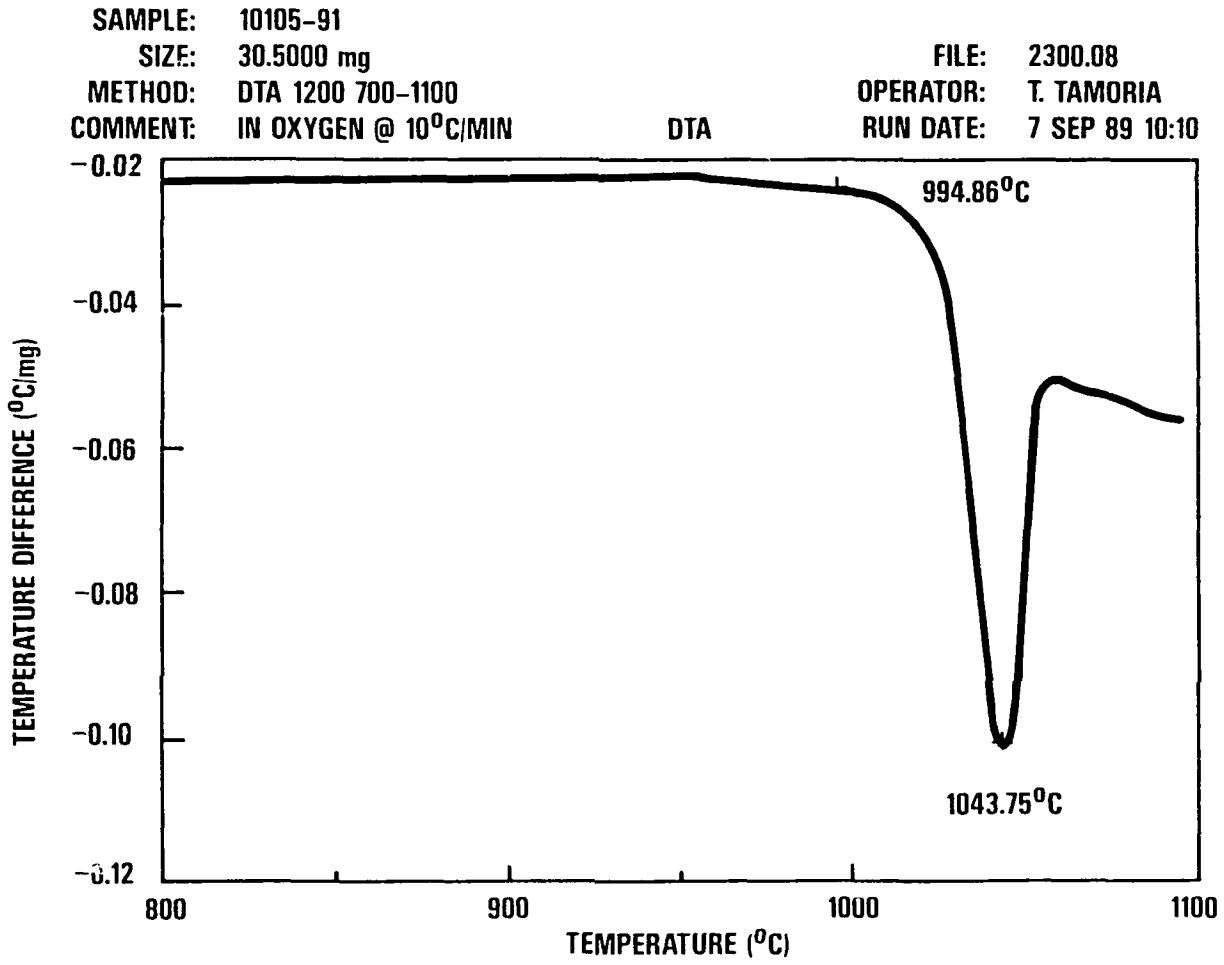

J-736(8)
9-25-90

Fig. A-12. DTA of the powdered 123 film sample with no evidence of low melting phase

J-736(6)
9-25-90

NOTE THE LARGE GRAIN IN THE LOWER LEFT HAND CORNER PARTIALLY OBSCURED BY ANOTHER GRAIN

Fig. A-13. TEM bright field micrograph of a sol-gel derived 123 thick film

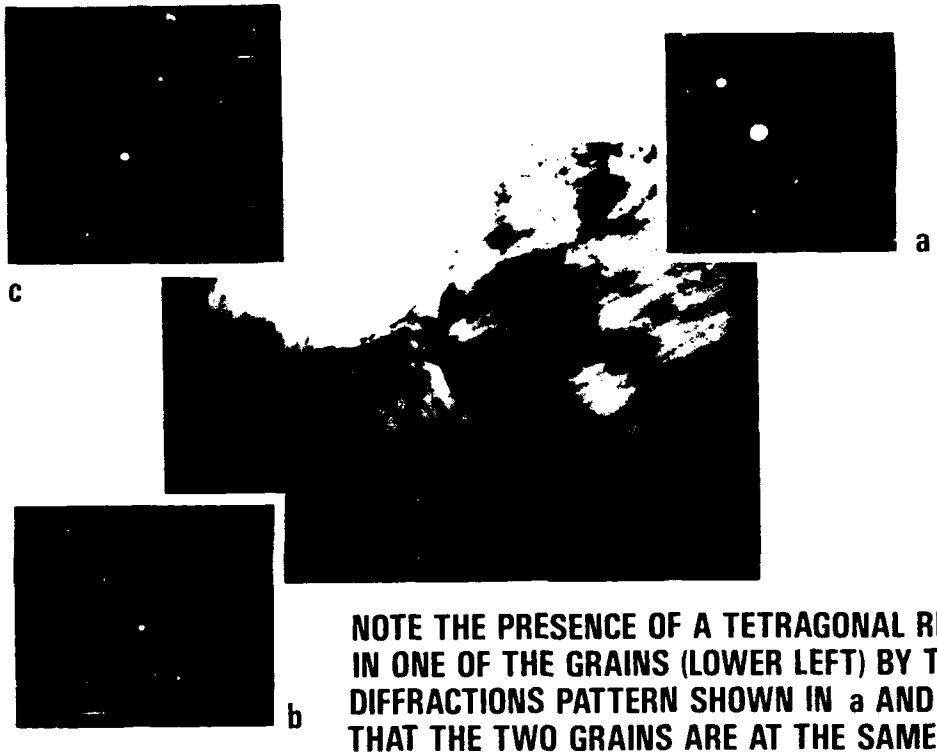

NOTE THE PRESENCE OF A TETRAGONAL REGION IN ONE OF THE GRAINS (LOWER LEFT) BY THE BOUNDARY. DIFFRACTIONS PATTERN SHOWN IN a AND b GRAINS INDICATE THAT THE TWO GRAINS ARE AT THE SAME ORIENTATION AS OPPOSED TO THE DIFFRACTION PATTERN SHOWN IN c

J-736(5)
9-25-90

Fig. A-14. TEM bright field micrograph showing a 3 grains junction

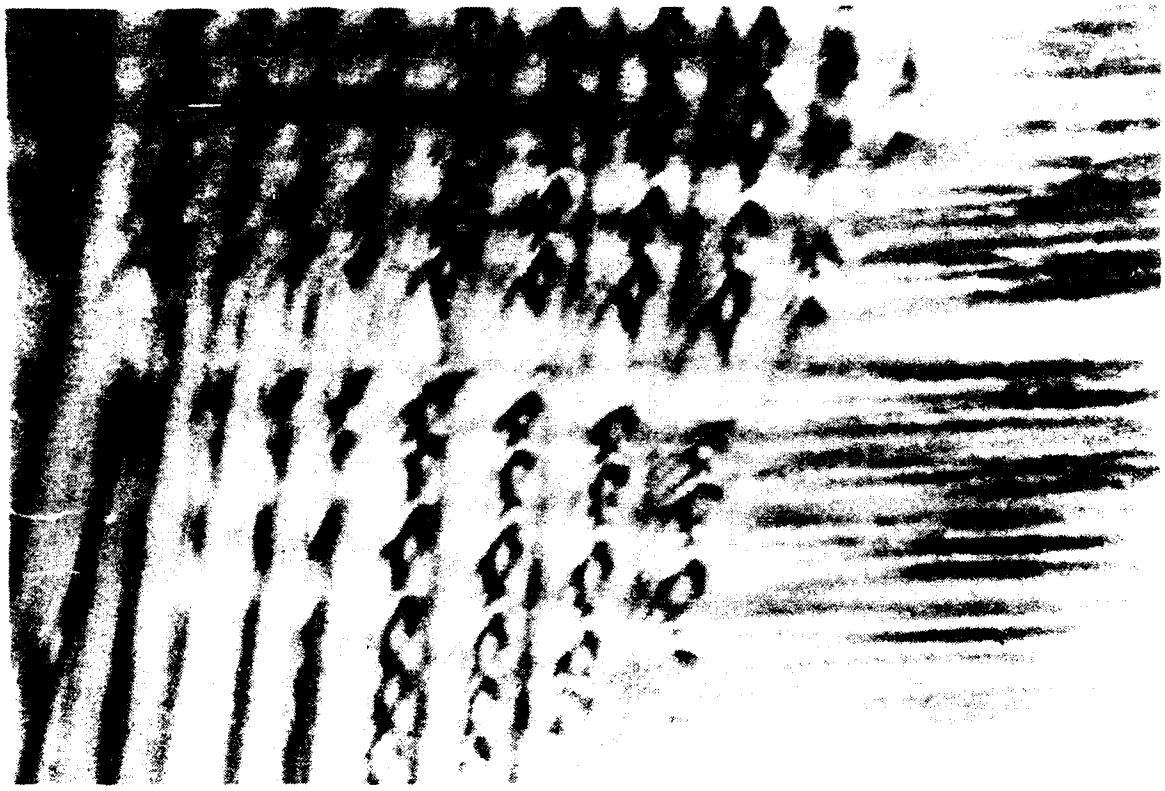

Fig. A-15. Cross twinning of orthorhombic grains

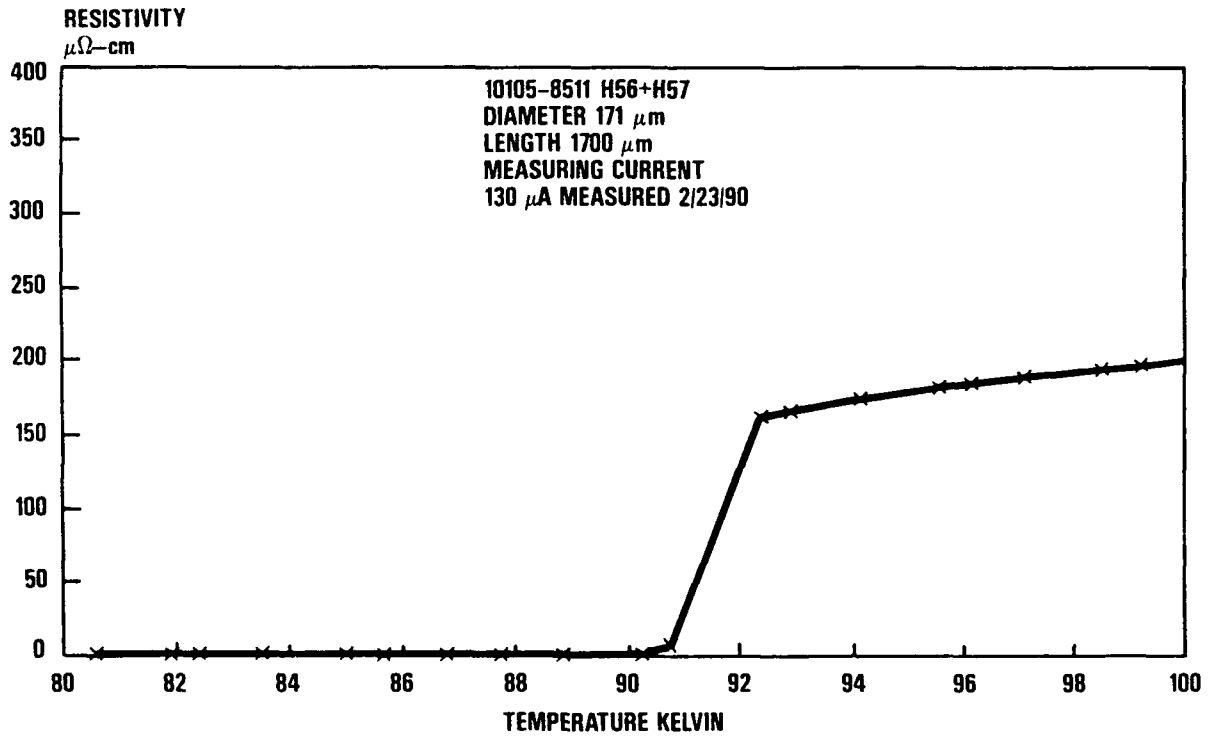

J-736(7)
9-25-90

Fig. A-16. Resistivity of the sol-gel derived 123 superconductor thick film

Some 211 phases were detected in the XRD patterns of both as-received powders but they disappeared after being calcined at 900°C for 8 h in O_2. However, for both powders, the DTA results did not show much difference between the as-received and after calcination, namely the powders contained some impurity phases and melting occurred above ~920°C.

A.3. IN-SITU PREVENTION OF BARIUM CARBONATE FORMATION BY MODIFICATION OF THE SOLUTION CHEMISTRY

During the course of this program, a method was developed to prepare a homogeneous stable solution that can be converted to viscous liquid or solid resin states for fiber drawing. Many associated chemistry problems, which influence the stoichiometry of the starting solution and phase purity in the final superconducting ceramics, have been successfully resolved. It was found that it is possible to control microstructure to incorporate minor 211 phase inclusions in the fibers by a slight adjustment in the solution stoichiometry at an early stage of the solution preparation. The solution chemistry was further improved to avoid stable barium carbonate formation. This has been accomplished by partial substitution of copper ethylhexanoate with copper trifluoroacetate.

In replacing of some of the copper ethylhexanoate with copper trifluoroacetate to provide four to six moles of fluorine per formula of Y123, it was discovered that no barium carbonate was found during the pyrolysis of the preceramic fibers. In these fibers, barium fluoride and copper oxide were found at intermediate temperature range [Fig. A-17(a)]. By calcining at 850° to 900°C in a flowing oxygen saturated with water, single phase Y123 was produced in these fibers [Fig. A-17(b)]. The optimal temperature and duration of heat treatment have not yet been established. These two parameters, together with the resulting microstructure, need to be evaluated for continuous fiber processing before the copper trifluoroacetate containing solutions can be adapted for the final fiber processing.

- **STARTING COMPOUNDS**

$$1\ Y(OP^{i}_{r})_3 + 2\ Ba\ (OP^{i}_{r})_2 + 2\ \frac{1}{3}\ Cu(EH)_2 + \frac{2}{3}\ Cu(CF_3COO)_2$$

- **REACTION SEQUENCE**

$$\text{AMORPHOUS} \xrightarrow[2\ HR]{500^{\circ}C} \begin{bmatrix} BaF_2 \\ CuO \end{bmatrix} \xrightarrow[900^{\circ}C,\ 12\ HR\ Dry\ O_2]{900^{\circ}C,\ 3\ HR\ WET\ O_2} \begin{bmatrix} 211 \\ BaF_2 \\ CuO \end{bmatrix} \xrightarrow[900^{\circ}C,\ 20\ HR\ Dry\ O_2]{850^{\circ}C,\ 18\ HR\ WET\ O_2} Y123$$

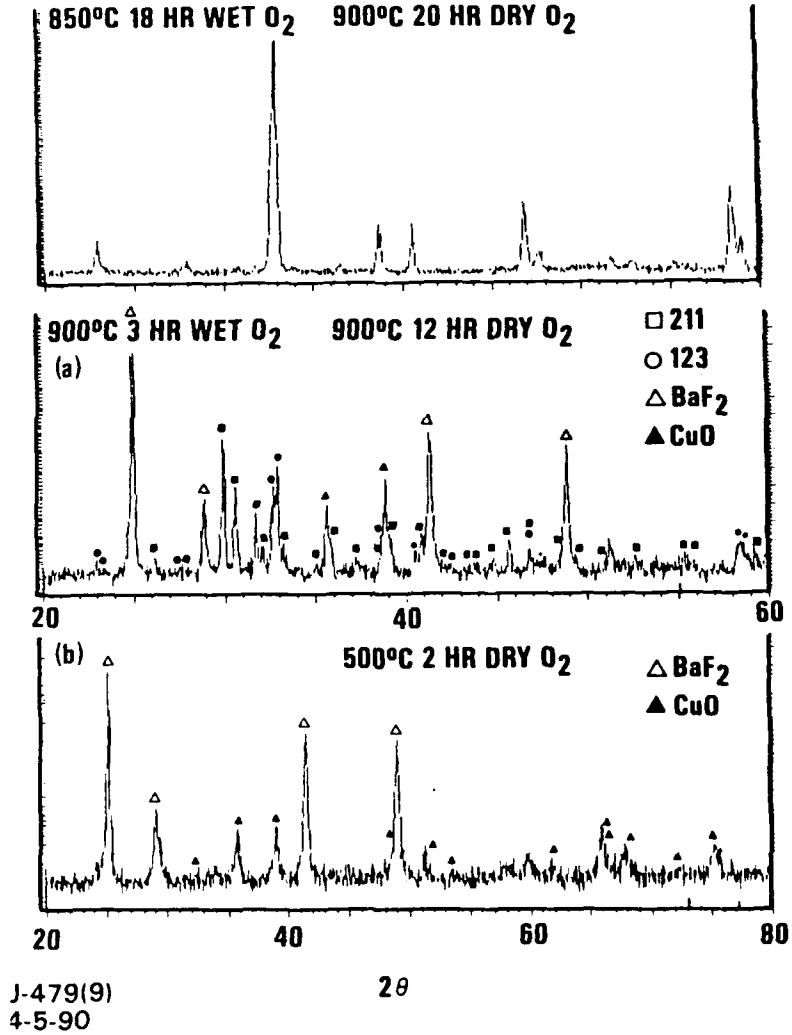

Fig. A-17. X-ray diffractions of fibers calcined at (a) 500°C for 2 h and (b) 850°C for 18 h in dry O_2 then at 900°C for 18 h in wet O_2 atmosphere

A.3.1. Effect of Solvent Mixtures on the Rheology Behavior of the Resin

It has been found that the rheology of the resin was strongly influenced by the presence of different kinds of solvents as well as their relative amounts. In certain combinations, a minute change in the solvent ratio has a profound influence on the viscosity. Therefore, the effects of the solvent concentration in the resin on the rheological behavior of the resin was closely examined. The purpose of this study is to define the volume fraction of solvent mixtures in the resin that are necessary to obtain a certain viscosity. Once the conditions are found, the resin can be readily converted to suitable viscosities for either film or fiber processing.

A.3.2. Behavior of the Y123 Resin in Benzene-Isopropaol Binary Solvents

First, the qualitative rheology behavior of the dry resin in different combinations of benzene and isopropanol was examined (Fig. A-18). In this ternary phase diagram, there are six major regions. In Region I, the resins are viscous, and the viscosity decreases with increasing amounts of benzene (e.g., point 1 is more viscous than point 2). Fibers or thick films are made within certain combinations of benzene and isopropanol within this region. However, on the tie line between the dry resin and toluene, resin is cohesive (Fig. A-19).

A.3.3. Behavior of the Y123 Resin in Xylene-Isopropanol Binary Solvents

The behaviors of resin in the toluene-isopropanol binary system have also been studied (Fig. A-20). As in the previous systems, there are also similar regions. A similar viscous range was found in the benzene-isopropanol system. There exists a much larger homogeneous solution region. On the tie line between the dry resin and toluene, the cohesive property of the resin is again observed. Two unique features of this system are that (1) the solution viscosity in the homogeneous

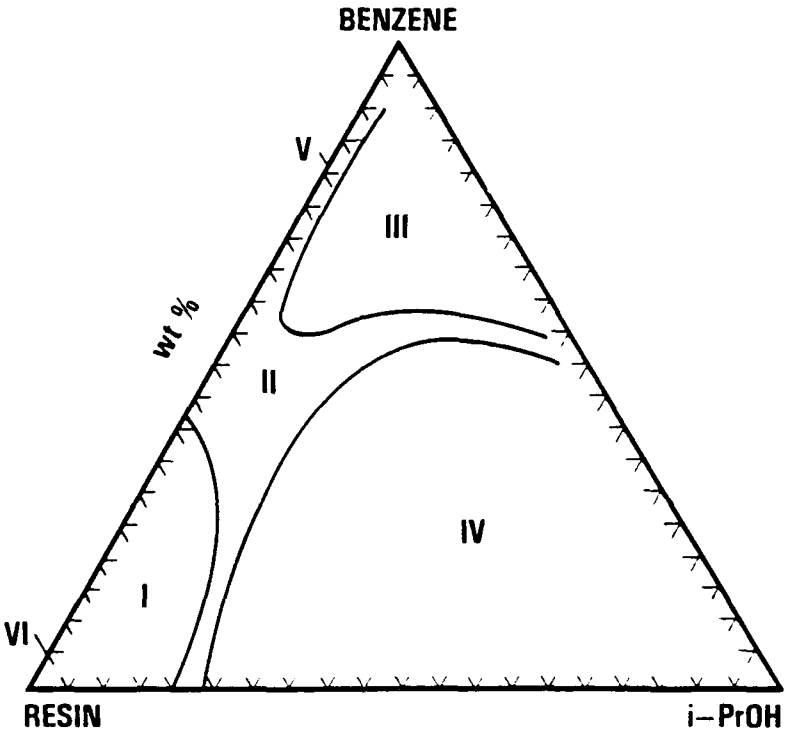

Fig. A-18. Characteristics of the Y123 resin in benzene-isopropanol binary solvents

J-481(6)
4-3-90

Fig. A-19. The cohesive property of resin in benzene enables it to be molded into different shapes

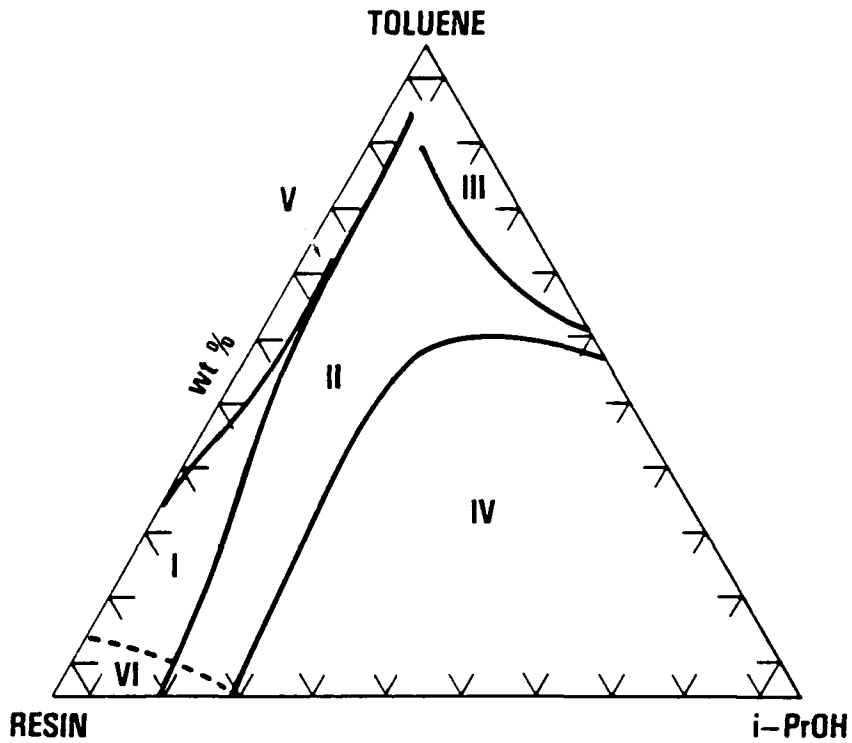

Fig. A-20. Characteristics of the Y123 resin in toluene-isopropanol binary solvents

region is higher than those homogeneous solutions in either benzene-isopropanol and toluene-isopropanol systems and (2) the evaporation rate of solvents is slightly slower. As a result, the xylenes-based solutions are better for thick film applications.

A.3.4. Behavior of the Y123 Resin in Binary Polar-Nonpolar Solvents

Four examples of typical binary polar-nonpolar-based system having similar wide range of homogeneous solutions, a large precipitation region, and a small viscous region located close to the apex of dry resin are shown in Fig. A-23.

A.4. RESIN SPINNING PROPERTIES AS A FUNCTION OF SOLVENT CONSTITUENTS

While it has been shown in the last annual report that the fiber can be continuously spun from these resin Fig. A-24, the refinement of the solvent content in the resin and its effect on spinning processes have not yet been examined. The spinning properties that are critical for continuous fiber spinning include the rheology and the plasticity of the resin, die-swelling of the resin, surface smoothness of the fiber after extrusion, drying rate and flexibility of the fiber, possible collapse of the fiber after solvent evaporation or deformation under its own weight, green strength, and pressure needed for extrusion. These must be examined concurrently or simultaneously before a process flow sheet is constructed.

While it is not conclusive at the present time which one of the viscous regions in the above four systems is better for the continuous spinning requirements, it was found that only a very narrow combination of solvents and resin in the viscous regions in each system is possible. As an example, some results in the benzene-isopropanol system are given in Table A-3.

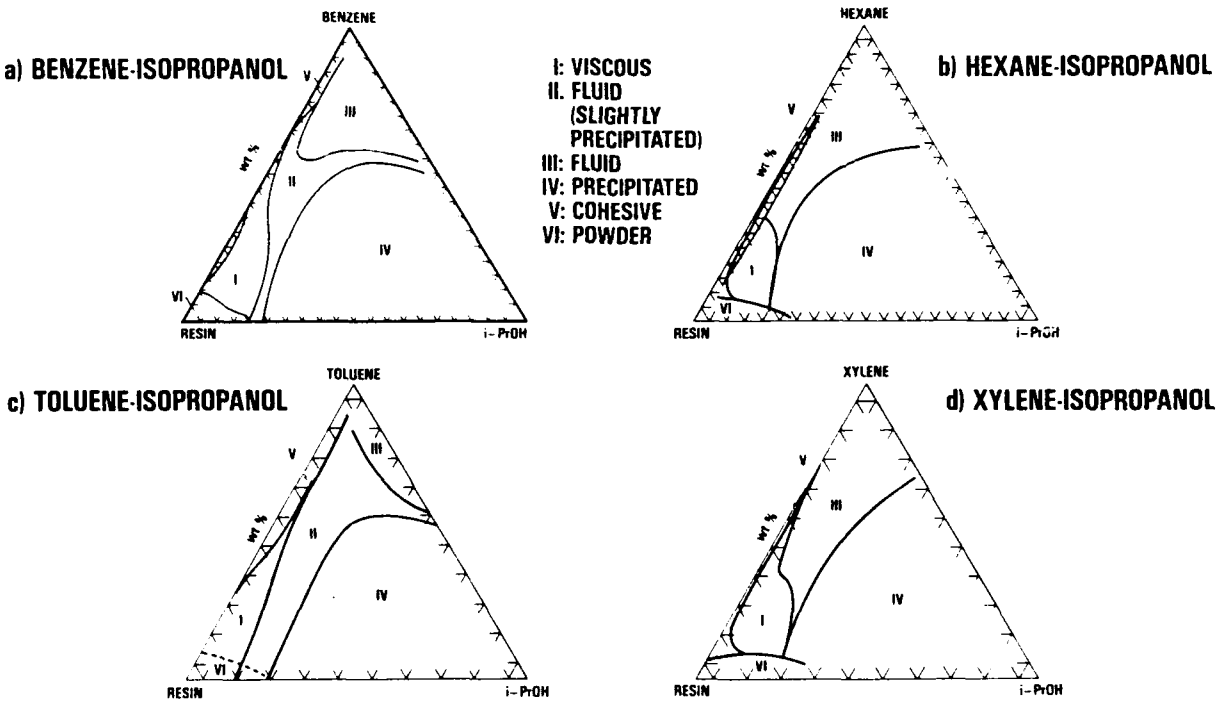

J-479(6)
8-16-90

Fig. A-23. The characteristics of Y123 resins in binary solvent systems

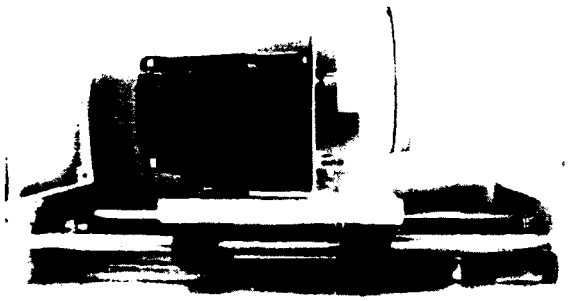

(a) DOWN-DRAWING SPINNING

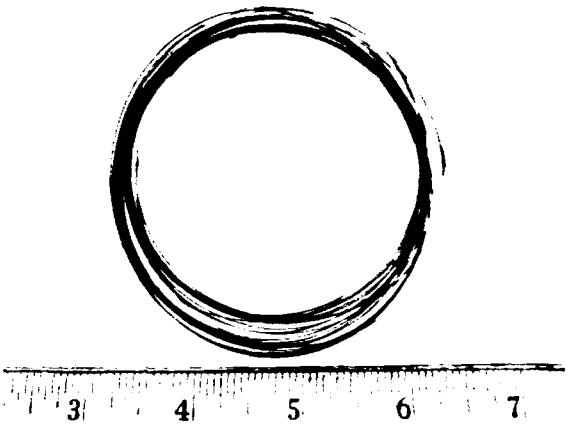

(b) CONTINUOUS PRE-CERAMIC YBCO FIBER

J-047(14)
9-25-90

Fig. A-24. Continuous preceramic superconductor fibers spun from the metallo-organic solution

TABLE A-3
SPINNABILITY OF RESINS IN BENZENE-ISOPROPANEOL COHESIVE REGION

TEST RUN	RESIN CONSTITUENTS (WT %)			RESIN CHARACTERISTICS				
	C_6H_6	i-PrOPH	DRY RESIN	COHESIVE	SURFACE SMOOTHNESS	DIE SWELL	FLEXIBILITY	COLLAPSE
B1	26.8	0.0	73.1	YES	NO	SLIGHT	SOME	NO
B2	48.3	2.6	49.1	YES	YES	SLIGHT	YES	YES
B3	39.6	2.2	58.3	NO	YES	LARGE	YES	YES
B4	25.4	1.4	73.2	YES*	YES	LARGE	YES	YES
B5	30.3	1.1	68.5	YES*	YES	NO	YES	YES
B6	20.0	1.0	78.9	YES*	YES	LARGE	YES	YES
B7	18.8	1.0	81.2	YES*	YES	NO	YES	SLIGHT
B8	17.8	1.0	80.2	YES	YES	NO	YES	NO

* SLIGHTLY TENACIOUS

J-481(7)
4-3-90

The effects of the solvent contents on the as spun fiber die-swelling and collapsing can be clearly seen in Figs. A-25(a) through A-25(d). In these samples, the amount of isopropanol were kept at 1 wt % and the amounts of benzene were slightly changed. The few percent variation in benzene gave rise to different degree of die-swelling and collapsing. The sample B5 had no die-swelling and a large collapsing and the sample B6 had a large die-swelling and a medium collapsing. The samples B7 and B8 had no die-swelling which is desirable. Another important property that had been examined was the draw-down ratio. This property enabled the fiber to be axially stretched to obtain smaller diameter fibers. Sample B9 demonstrated a resin with a high draw-down ratio. The fibers were stretched to obtain a smaller diameter fibers. Sample B9 demonstrated a resin with a high-down draw ratio. The fibers were stretched to 1/5 to 1/6 of the diameter of the nozzle.

While the effects of solvent constituent was clearly shown, the relation and the relative importance of the die-swelling, collapsing, and drawn-down ability are still unclear. For example, from a processing point of view, a resin with large die-swelling which has a large draw-down ratio may be as good as a resin with no die-swelling and small draw-down ratio. Further studies will be performed in this area to clarify this issue.

A.4.1. Heat Treatment Schedule Study

The spun fibers had a relatively uniform diameter along the fiber length. However, the diameter of the as-spun fibers were 200 to 500 microns which were thicker than those previously reported of hand-drawn fibers with 50 to 200 microns in diameters. The larger diameters in the spun fibers poses a stringent requirement on heat treatment schedule. Therefore, the current practice is to spin a thinner fiber and, at the same time search for a new heat treatment schedule for thicker fibers. To refine the heat treatment process parameters for

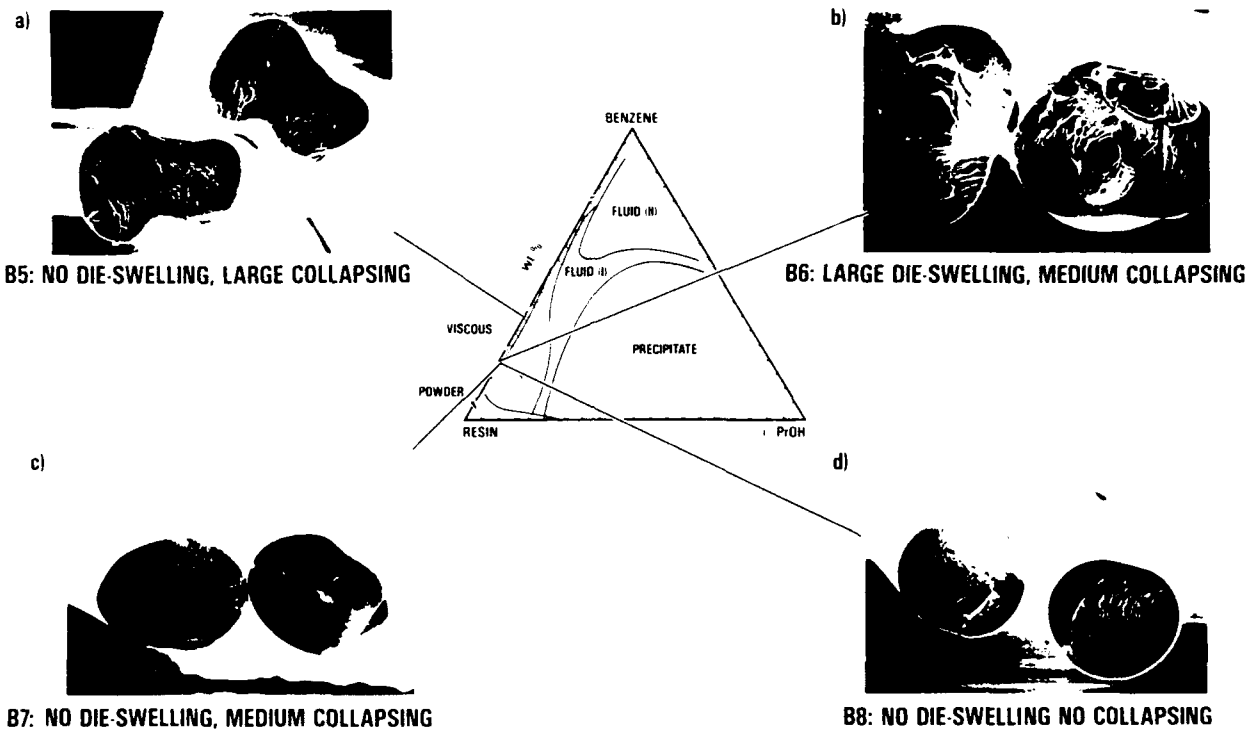

J 735(5)
9 25 90

Fig. A-25. Precursor fibers morphology with different degrees of die-swelling and collapsing

these fibers, it was necessary to do iterative processing of the same fiber lot at different times and temperatures schedule. It was found that the first critical stage of the heat treatment was the organic removal and/or burn out between 200° and 350°C. The improper organic pyrolysis through this temperature range invariably resulted in axial crackings and weak fibers (Fig. A-26). Based on the careful TGA of the resin, several promising heat treatments in the range of 100° to 450°C were attempted. The polished cross sections of the fibers heat treated at a specific schedule indicated no axial cracks.

The superconducting properties were evaluated by using dc magnetic susceptibility on the short fibers, and resistivity and current density measurements on longer fibers. The electrical properties of the fibers were found to be strongly dependent on the high temperature heat treatment. The superconducting onset temperature of these fibers was improved from previously reported 87 to 92.5 K and zero resistance temperature from 81 to 90 K. (Detailed superconducting properties of the fibers are described under the electromagnetic properties characterization.)

A.2.2. Improvement of Fiber Current Density

Sol-gel derived fibers of 123 with T_c of 90 to 91.5 K and ΔT = 1.5 to 2 K were prepared in accordance with the flow diagram (Fig. A-4). However, the current density of the fibers were only in the range of 50 to 200 A/cm^2. Therefore, during the last year, major emphasis was placed on improving the current density of these fibers.

The low current density in the fibers were believed to be due to undesirable microstructure, which includes cracking, large grain size, large size porosity, and second phases. The problem of axial cracking usually occurred during the low temperature (200° to 400°C) organic pyrolysis has been solved by using a stepwise heat treatment schedule as described previously. The curing pyrolysis schedule requires 3 days

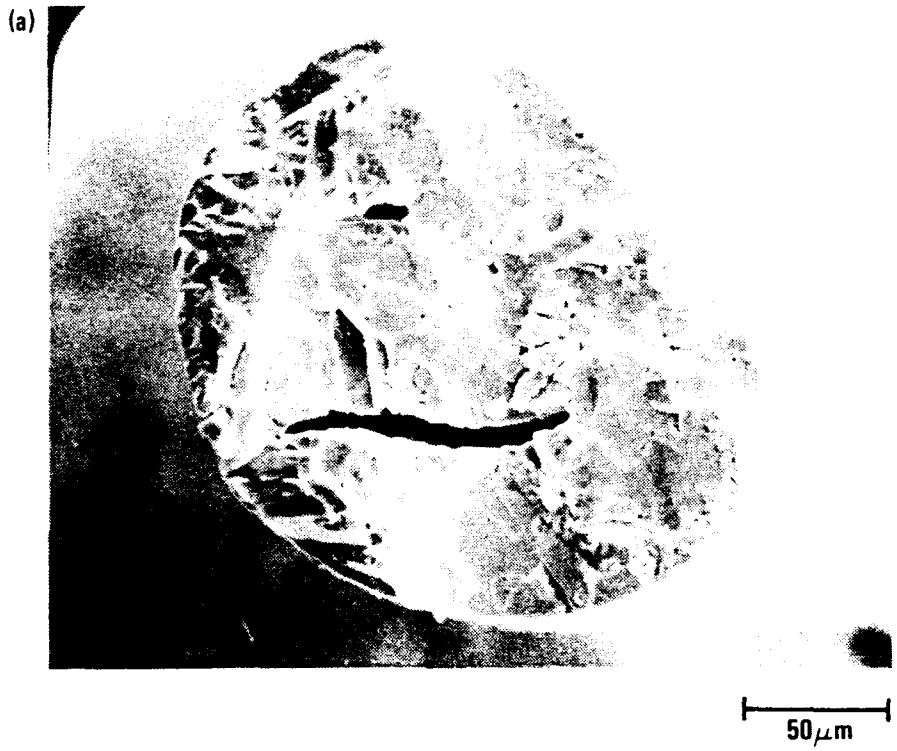

Fig. A-26. Fracture surface of the axially cracked fiber sintered at 935°C, 24 h, and 950°C, 5 h (Sample 10105-91 H51)

to allow the organic pyrolysis by-products to diffuse out from the interior of the fiber. At the present time, fibers without axial cracking are routinely obtained. While the improvement of the heat treatment schedule is still being investigated, mainly to shorten the heat treatment schedule, in order to streamline the processing time and to test heat treatment reliability, it was discovered that the axial cracking was not the major cause of low current density.

Examining the microstructure of the polished crossed sections of the fibers, we found that the grain size (randomly oriented) of the fibers were too big so that it is possible that the major part of the current flow in the fiber is limited by only a few number of big crystals of unfavorable orientation. The large grain size in the fibers can be clearly seen by using a polarized optical microscopy [Figs. A-27(a) and A-27(b)]. The large grain size in the fiber was partially due to the prolonged time and higher temperature used in an attempt to densify the fiber and also due to very slightly off-stoichiometry from 123 composition in the fiber. The fibers made from the batch 10105-85 II having a finer grain size as compared to the fibers from batch 10105-91 was attributed to a very slight composition fluctuation noting that both are DTA pure. The smaller grain size of batch 10105-85 II is shown in Fig. A-28(a). A significant amount of porosity was also observed indicating further densification would increase the current density [Fig. A-28(b)].

The experimental results indicate that in order to improve current density of the 123 fibers, it is imperative to improve the microstructure of the fibers. In an attempt to do that, first the maximum sintering condition was adjusted from 950°C for 24 h to 915°C for 24 h to reduce the grain growth during sintering. The grain size became smaller with decreasing temperature as shown in Fig. A-29(a). However, the density of the fibers decreased as more pores were observed [Fig. A-29(b)]. With a smaller grain size however, the average current density of three different samples measured were increased average to approximately 1000 A/cm^2 (944, 1100, and 1220 A/cm^2).

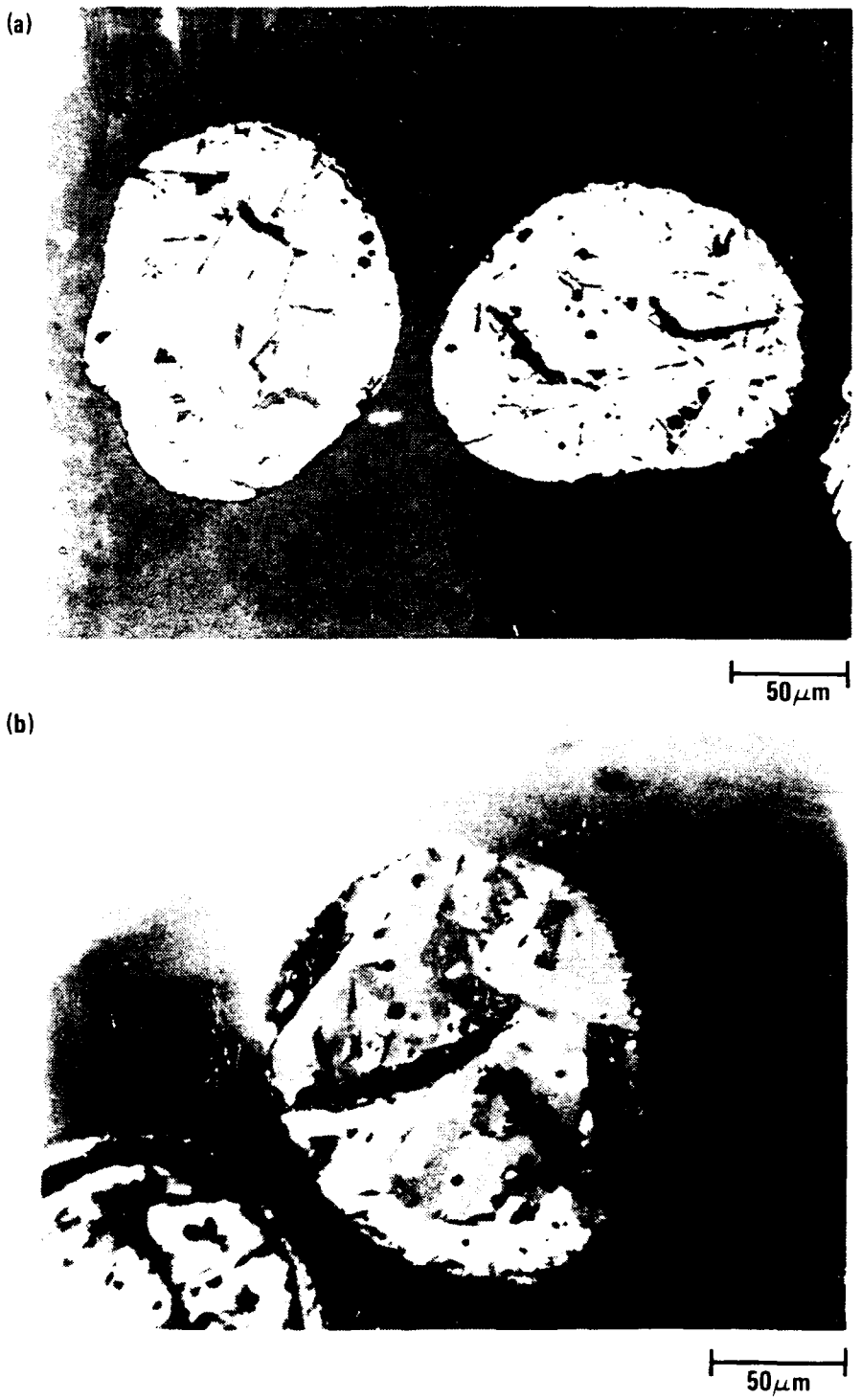

Fig. A-27. (a) The polished cross section of fiber showing large grain size and porosity (10105-91 H51; optical microscope 300X); (b) under polarized light to clearly reveal grain size (400X)

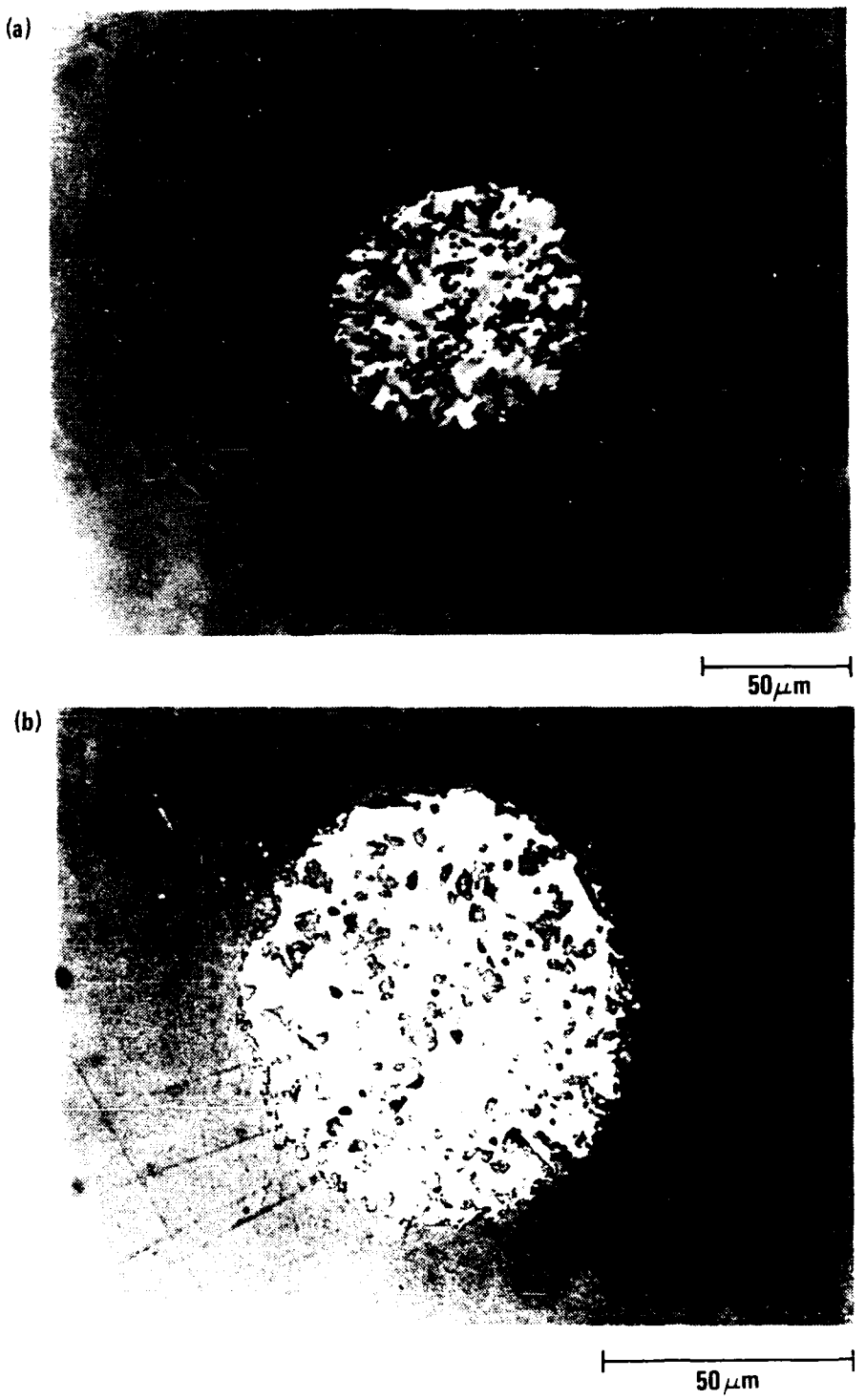

Fig. A-28. (a) The optical micrograph of the polished cross section of fiber from batch 10105-85 II calcined at the same maximum temperature (935°C, 24 h, 950°C, 5 h) showing finer grain size under polarized light (400X); (b) unpolarized light to show porosity (700X)

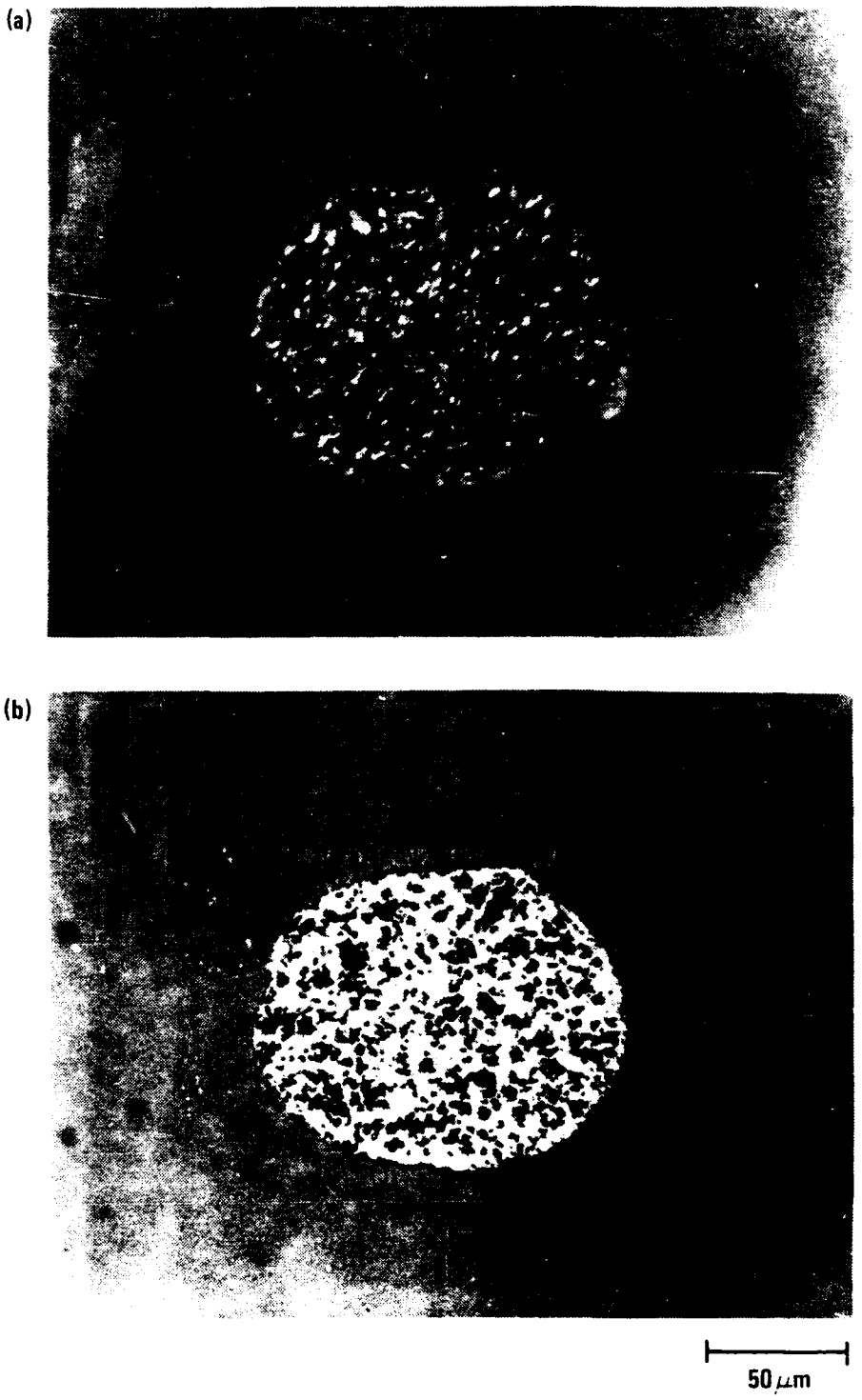

Fig. A-29. (a) The optical micrograph of the polished cross section of fiber calcined at 915°C, 24 h showing finer grain size (polarized light; 400X; J_c = 1100 A/cm^2); (b) unpolarized light to show a large amount of porosity (400X)

To enhance the densification, it was decided to add 3 wt % 0.4 μm in diameter silver powder to the resin. The uniform fine distribution of the silver particles in the spun fiber after organic removal can be clearly seen in Fig. A-30. Different temperature-time schedules were used to study the effect of silver addition on the densification of the fibers. Figure A-31 shows a decrease in the porosity with silver addition even though the maximum sintering temperature was decreased and the holding time was shortened [compared to Fig. A-28(b)], the grain size was still considered too big. Figure A-28 shows the cross section of the fiber with the sintering temperature lowered to 915°C for 12 h. The overall porosity increased but the pore sizes were smaller and more evenly distributed when compared with Figs. A-28(b) and A-29(b). Prolonging the sintering time at 915°C to 24 h, the porosity remained the same but the grain size remained small [Figs. A-32(a) and A-32(b)]. The current density of the fiber was improved and was in the range of 1400 ± 600 A/cm^2. A maximum current density of 2083 A/cm^2 was observed (77 K, zero field). It should be noted that further reduction in sintering temperature to 900°C for 24 h, decreased the current density of the fiber to 200 A/cm^2 with porosity remaining at the same level, Fig. A-33. Detailed critical current density measurement on the fibers made are described under the electromagnetic properties characterization Section 3.1.

Based on the current density measurement, it is apparent that by improving the microstructure, it may be possible to double the fiber current density if fiber can be densified without excessive grain growth. In order to increase the current density further, the grain alignment of the fiber is the next essential step. The microstructure texturing of the fiber is in progress.

A.2.3. Reduction of the Fiber Shrinkage During Sintering

As mentioned previously, another obstacle for continuous processing of the sol-gel derived 123 fiber is that the fibers have a large dimensional shrinkage (approximately 50%) during sintering. In order to

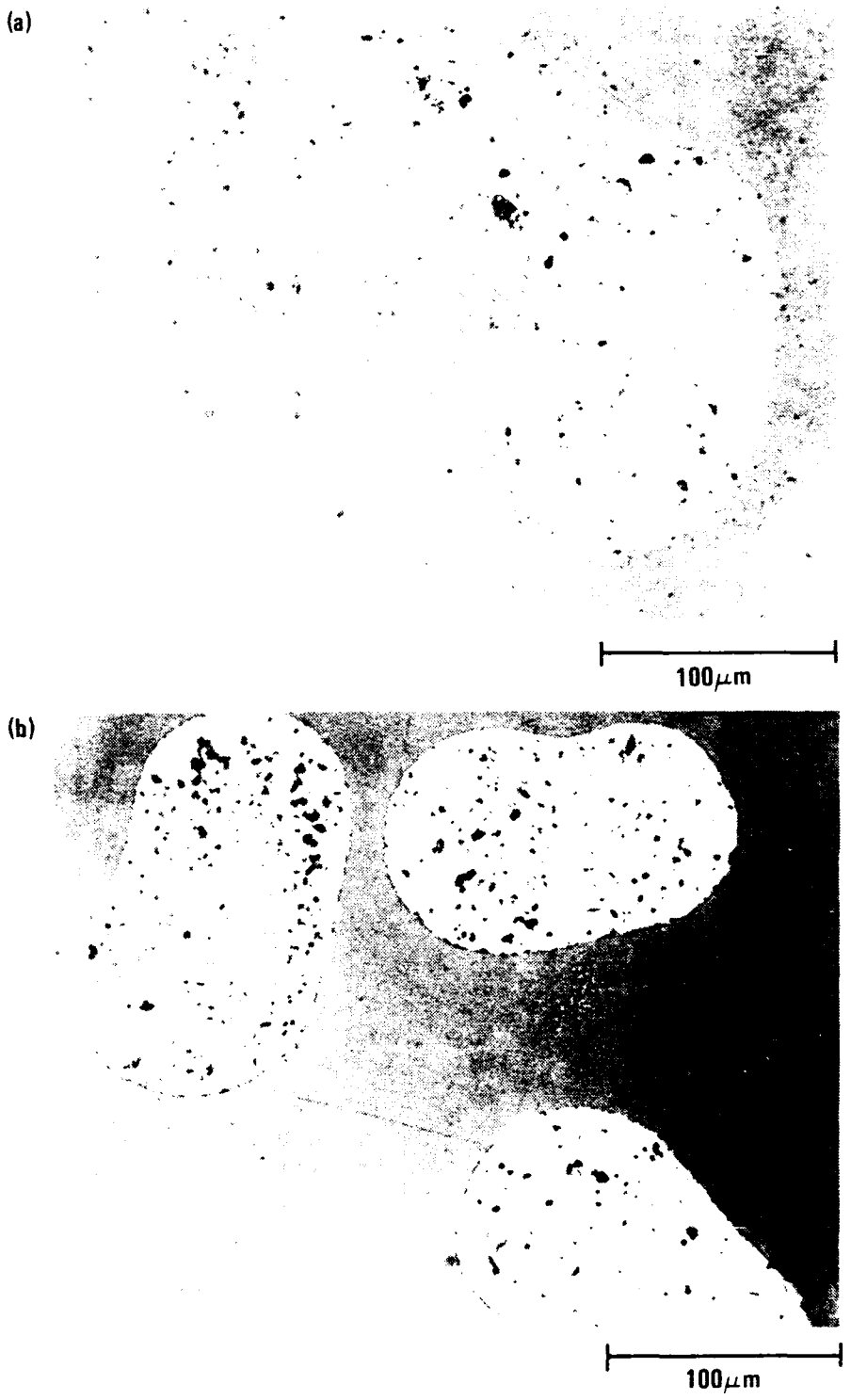

Fig. A-30. (a) The fiber with fine silver powder (3 wt % after calcination) showing silver particles are well-distributed (Sample 10105-85 II (Ag)-H66, 475°C max calcination, 300X); (b) the polished cross section of silver-added fiber sintered at 920°C, 18 h and 935°C 5 h showing decrease in porosity (Sample 10105-85 II (Ag)-H72; 300X)

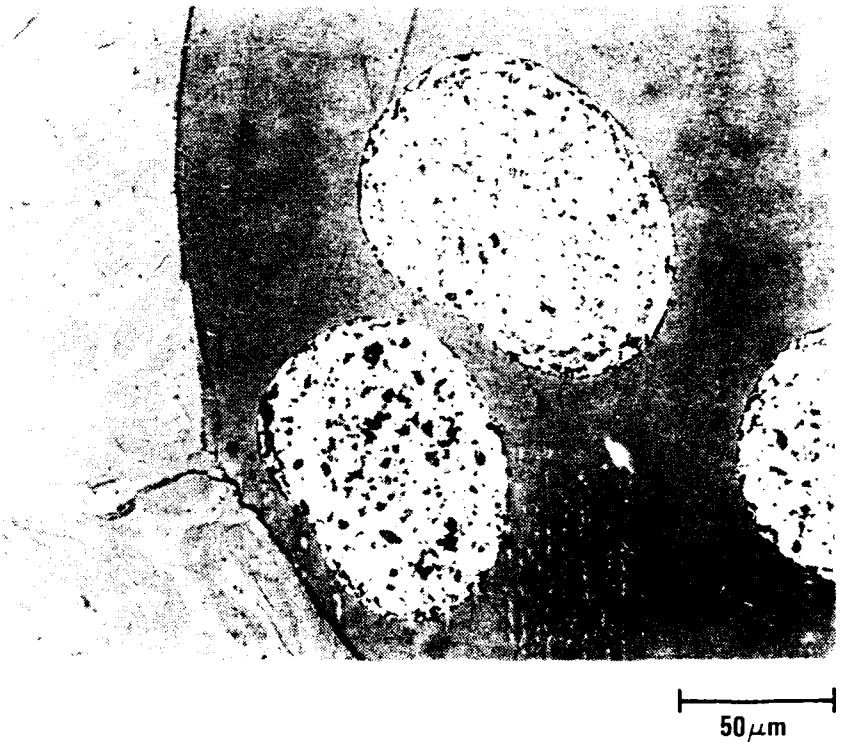

Fig. A-31. Optical micrograph of the polished cross section of the silver-added fiber sintered 915°C, 12 h showing porosity (Sample 10105-85 II(AG) H77,78; 400 X)

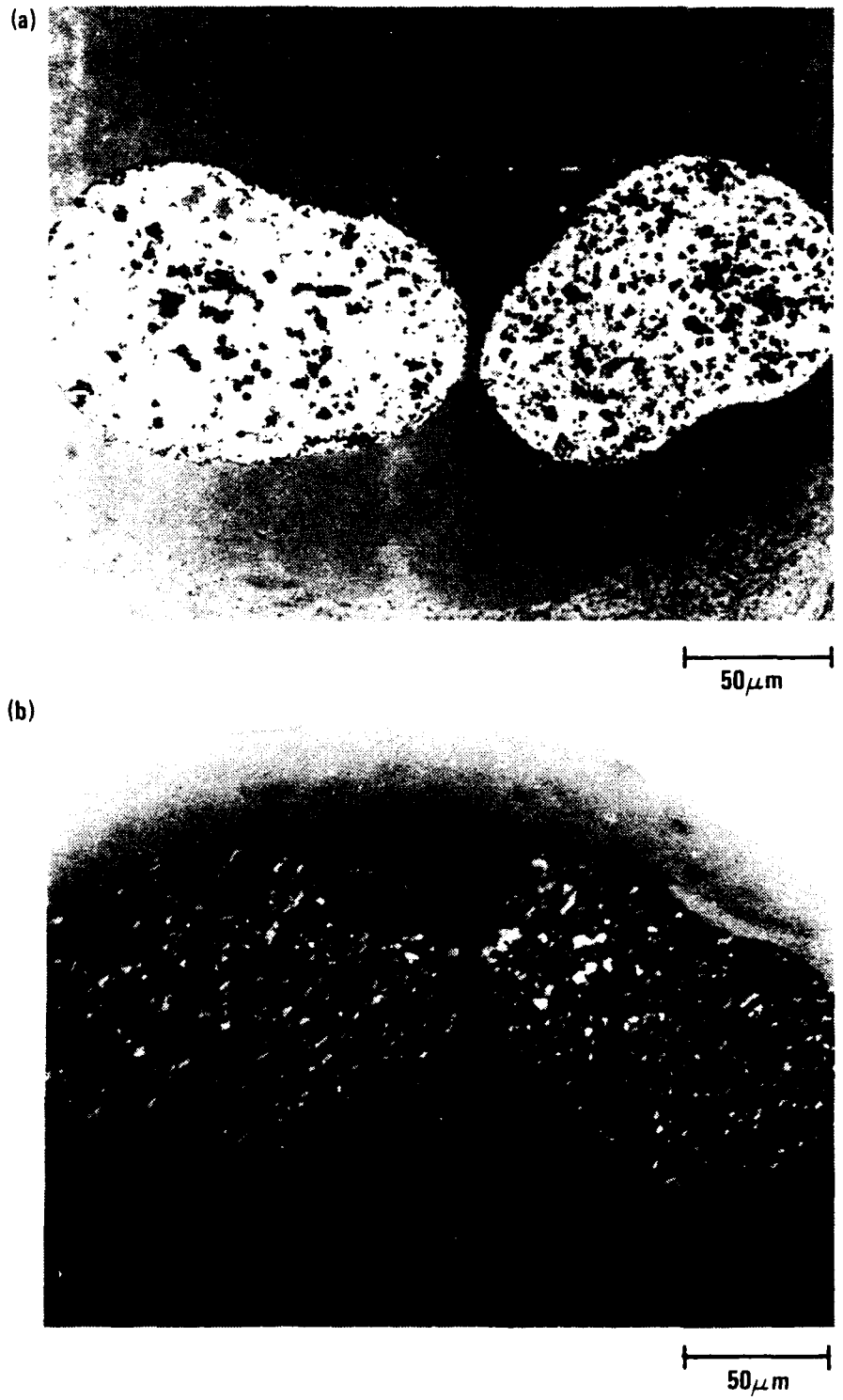

Fig. A-32. (a) The polished cross section of fiber sintered at 915°C, 24 h showing porosity (Sample 10105-85 II(Ag) H70, 75, 57; 400X); (b) under polarized light to clearly reveal fine grain size (400X; J_c = 1000 to 2100 A/cm^2)

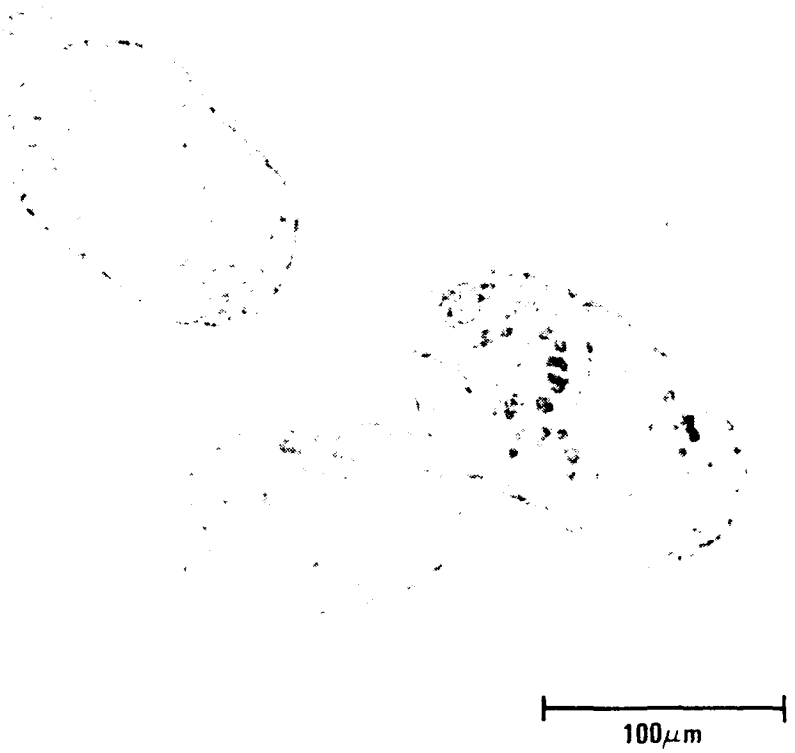

Fig. A-33. The optical micrograph of the polished cross section of fiber from batch 101056-85 II(Ag) sintered at the 900°C, 24 h showing a large amount of porosity (Sample 10105-85 II (Ag) H70, 71, 57; 300X; J_c = 201 A/cm^2)

continuously sinter the fiber as it is spun from the spinneret, it is necessary to reduce the shrinkage. The shrinkage can be reduced by adding some fine Y123 powder to the resin. A 30 wt % of fine Y123 powder (provided by Argonne National Laboratory) was mixed with resin powder together with 3 wt % of fine silver powder. This addition of 30 wt % Y123 powder reduced the shrinkage from the original 50% to approximately 41%. The addition of Y123 powder, however, has an adverse effect namely it has a tendency to decrease draw-down ratio which results in a thicker fiber. Currently, the amount of Y123 powder addition to the resin is being optimized.

Preliminary results indicate that with the same heat treatment condition at 915°C for 24 h, the fiber has slightly bigger grain size as compared with fibers with no Y123 powder addition [Figs. A-34(a) and A-34(b)]. The fibers also exhibit current density up to 1920 A/cm^2.

A-3. ELECTROMAGNETIC PROPERTIES OF SOL-GEL DERIVED MATERIALS

A variety of electromagnetic property measurements, including dc magnetic susceptibility as a function of temperature, electrical resistivity as a function of temperature, and transport critical current density, have been performed routinely on fibers and films prepared by sol-gel processes. In addition, a number of samples have been characterized by X-ray diffraction analysis, scanning electron microscopy, and electron microprobe analysis.

Electrical resistivity was measured at UCSD using a Linear Resistance LR-400 four-wire ac resistance bridge. Data were recorded with three Keithley 177 digital multimeters interfaced to an HP-85 computer. The current used for the measurements in this report was 1 μA.

Magnetic measurements were performed at General Atomics on a Quantum Design MPMS SQUID susceptometer.

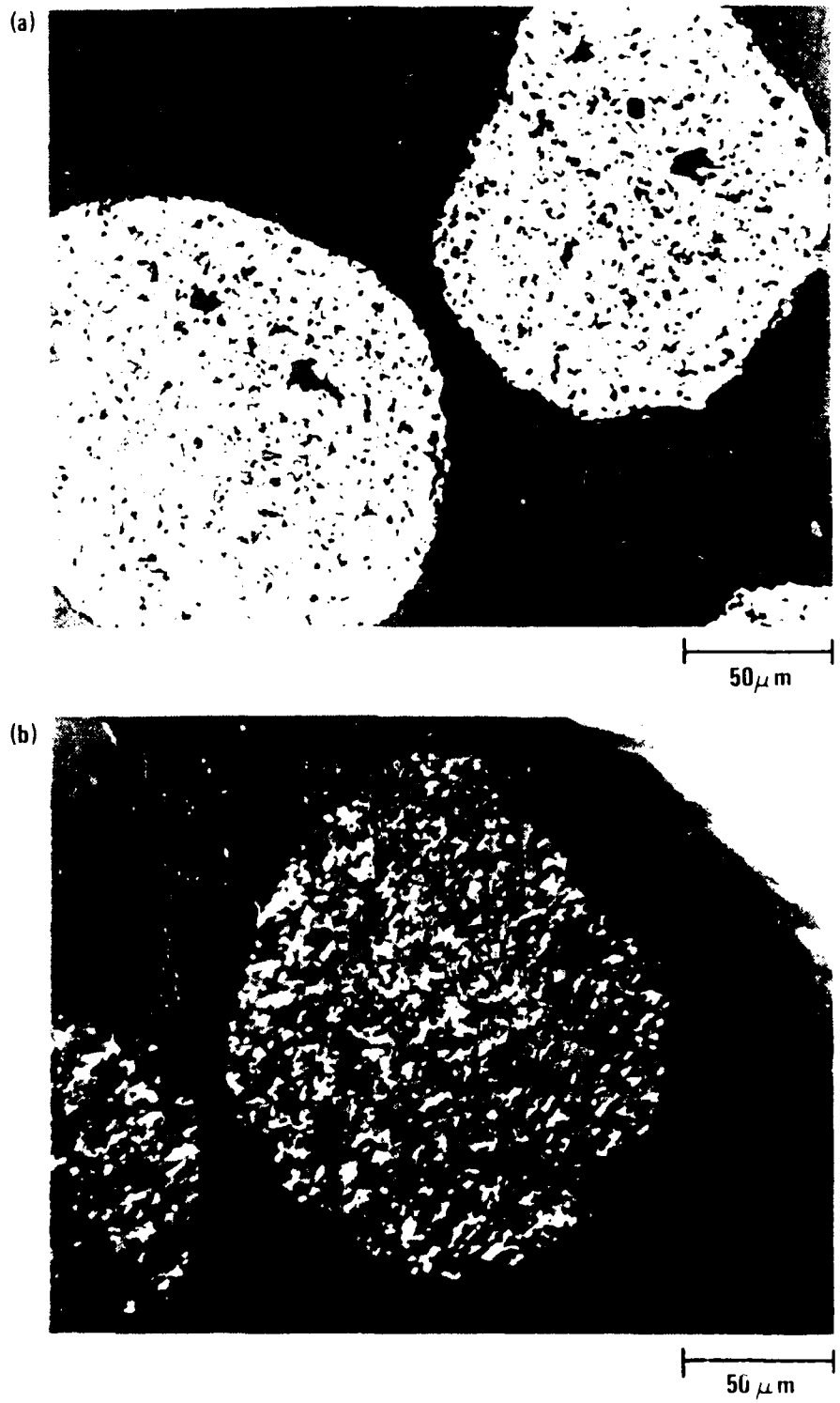

Fig. A-34. (a) Polished cross section of fiber with Y123 powder and silver addition with J_c = 1920 A/cm^2 using a nonpolarized light to show porosity and (b) polarized light to reveal grain size (400X)

Critical current was measured at UCSD in the absence of an applied field. Measurements were made using a four-wire dc technique with the sample immersed in liquid nitrogen. Equipment used included two Keithley 195A digital multimeters interfaced to a PC-AT compatible computer, a Kepco BOP 20-20M bipolar operational power supply and amplifier, and a Sorenson SRL 10-100 power supply. The critical current was determined using a criterion of 1 μV per cm as the voltage drop across the voltage leads.

Critical current was also measured as a function of temperature and applied field in a closed cycle refrigerator with He exchange gas at General Atomics using a four-wire ac technique. The cryostat, model 257171A manufactured by APD Cryogenics, Inc., was equipped with an APD HC-2 compressor. The electromagnet, HV-7A, and power supply, HS-1356 4A, were manufactured by Walker Scientific. Equipment also included a Tektronic 5223 digitizing oscilloscope, a Tektronix FG 501A 2 MHz function generator, a Tektronix 016-0597-00 trigger generator, a Stanford Research SR560 low noise preamplifier, a Lakeshore DRC82C temperature controller, and a Kepco BOP 20-20M power supply. Again, the critical current criterion was a voltage drop of 1 μV per cm separation between voltage leads.

Other analytical equipment used at UCSD included a Rigaku Rotaflex RU-200B X-ray diffractometer, a Cambridge 360 scanning electron microscope, and a Cameca Instruments CAMEBAX electron microprobe. The standard used for determination of sample composition by electron microprobe was a polished polycrystalline sample whose superconducting properties were well established to be those of $YBa_2Cu_3O_{7-\delta}$ and whose composition had been compared to a single crystal of $YBa_2Cu_3O_{7-\delta}$.

A.3.1. Fibers

Fibers of $YBa_2Cu_3O_{7-\delta}$ have exhibited consistently high superconducting transition temperatures as measured by dc magnetic susceptibility and electrical resistivity. A summary of the electromagnetic

measurements made on the $YBa_2Cu_3O_{7-\delta}$ fibers appears in Table A-7. The maximum critical current density measured in liquid nitrogen in zero applied field was 2100 A/cm^2 (Fig. A-35), and typical values were around 1000 A/cm^2. As shown in Fig. A-36, the critical current density of a fiber doped with 3 wt % Ag was also measured as a function of temperature from 20 to 77 K in zero applied field and at H = 100 Oe. The Ag dopant allowed the fiber to be drawn finer, while maintaining a critical current density of 950 A/cm^2 at 77 K in zero applied field. At 21 K, J_c attained a value of 7500 A/cm^2 for H = 0, and a value of 880 A/cm^2 for H = 100 Oe. The fiber used in these measurements had a diameter of 0.015 cm, and the separation between voltage leads was 0.183 cm.

A.3.2. Thin Films

Thin films of $YBa_2Cu_3O_{7-\delta}$ were made by two methods. In the first, the solvent is based on 2,2-ethoxy ethanol. The second method, which is potentially more cost-effective, uses a solvent based on toluene-isopropanol. Results are summarized in Table A-8. Critical current densities are derived from order-of-magnitude estimates of the film thickness. Because zero resistance was achieved below liquid nitrogen temperature, J_c was measured at 30 K in zero applied field.

The first processing technique yielded more reproducible results. The best superconducting properties were obtained for films dipped on large-grained yttria-stabilized zirconia substrates and annealed in flowing O_2 at 921°C for 1 min and at 405°C for 24 h. As shown in Fig. A-37, these films had high transition temperatures, $T_c = T_{50\%}$ = 91 K and narrow transition widths $\Delta T = T_{90\%} - T_{10\%}$ = 4 K as determined from electrical resistivity measurements. Transport critical current measured at 30 K in zero applied field was ~300 A/cm^2. X-ray diffraction showed some c-axis orientation. Electron microprobe analysis was performed on a number of thin films produced by this technique; considerable variations were found in the composition. Measurements of magnetic susceptibility were ambiguous, possibly because the films were too thin or because of small grain size.

TABLE A-7
$YBa_2Cu_3O_7$ FIBERS BY SOL-GEL METHOD
(Summary of Electromagnetic Measurements)

T_c[a]	$T_{50,\rho}$ = 91.5 K ΔT_ρ = 1.5 K
	$T_{onset,\chi}$ = >90 K $T_{50,\chi}$ = 87 K ΔT_χ = 10 K χ_{fc}/χ_{zfc} = 0.31
J_c(0G, 77 K)[b]	typ. 10^3 A/cm^2 max. 2.1 x 10^3 A/cm^2
J_c(H,T)[c]	See Figs. A-24 and A-25

[a]Reported first quarter 1990.

[b]Measurement performed in LN_2.

[c]Measurement performed in He vapor.

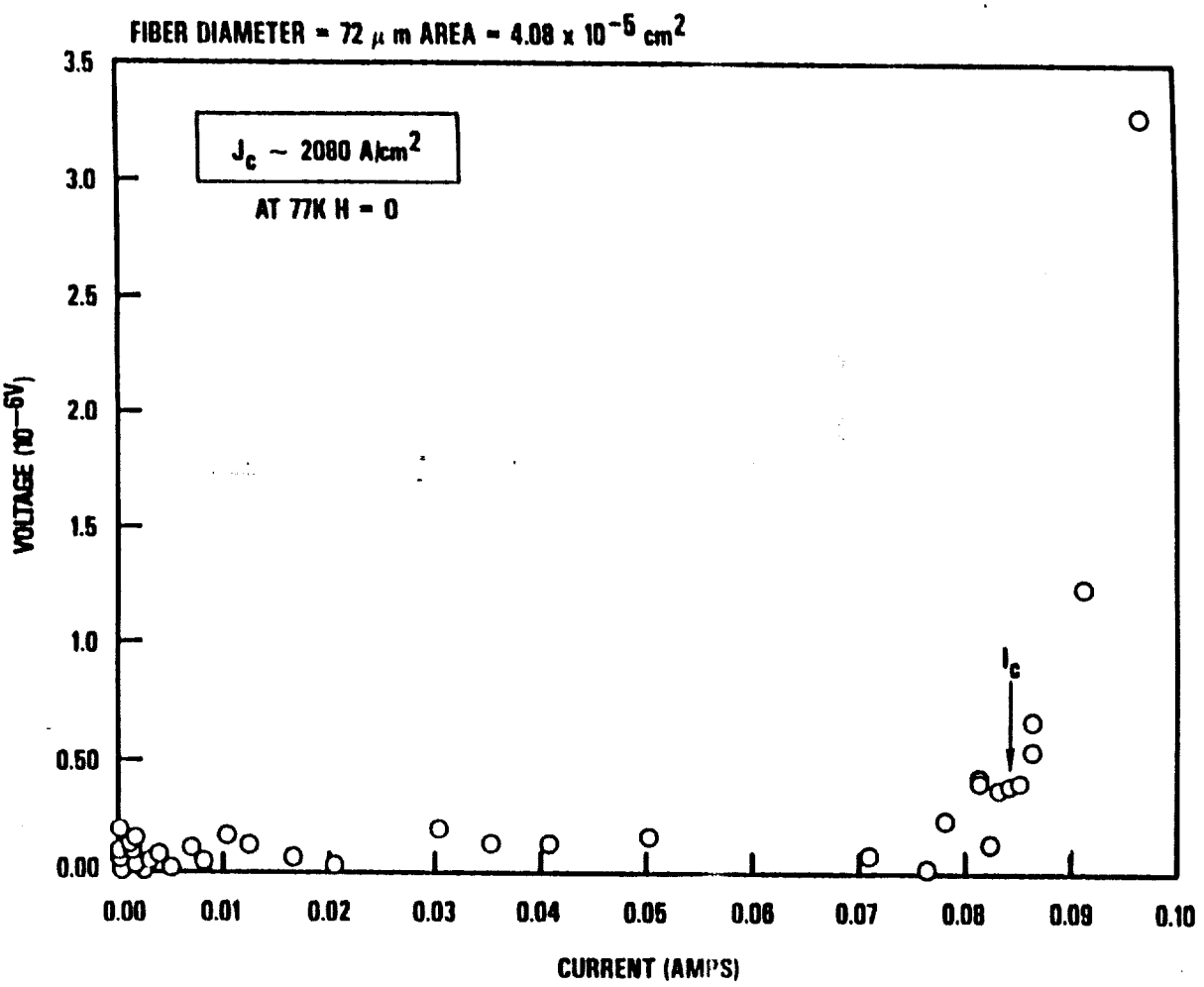

J-742(1)
9-28-90

Fig. A-35. Critical current density of sol-gel derived YBCO superconducting fiber

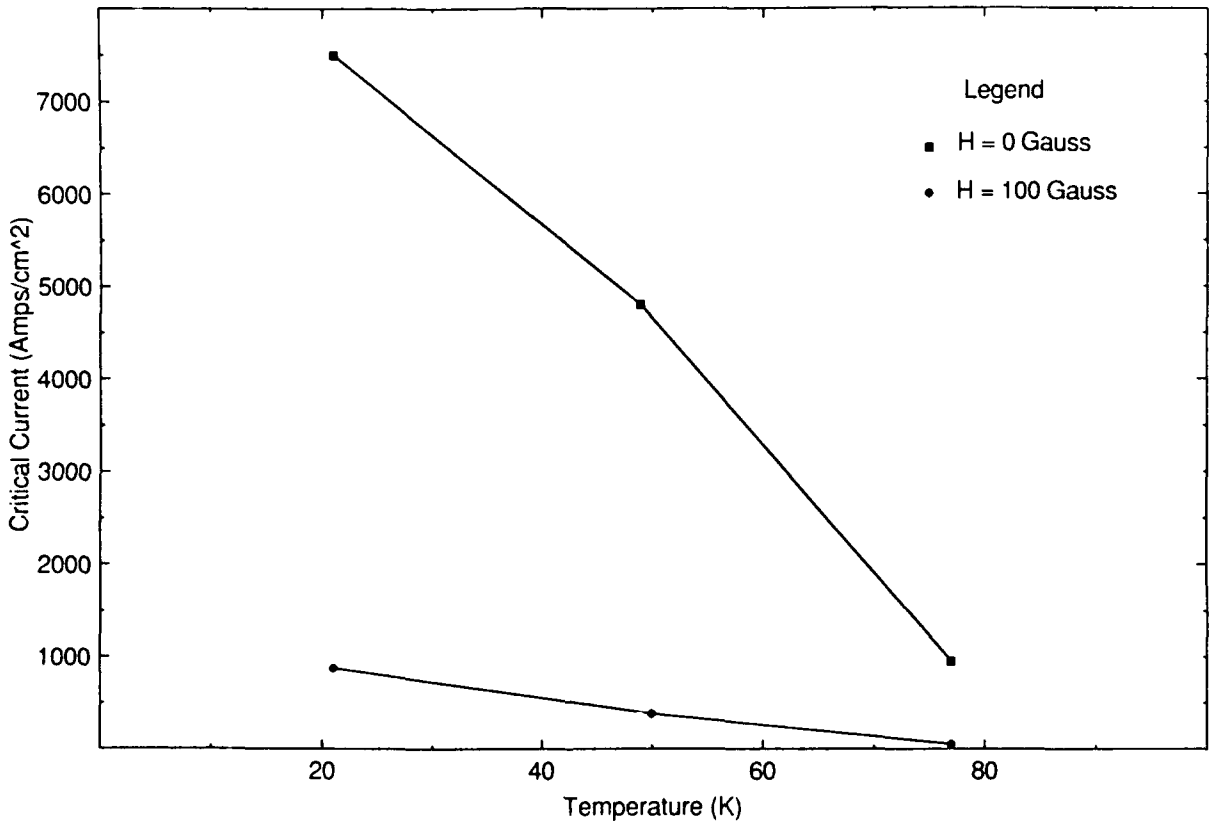

Fig. A-36. Critical current density as a function of temperature for an $YBa_2Cu_3O_{7-\delta}$ fiber at zero applied field and at H = 100 Oe. The fiber was doped with 3 wt % Ag. The critical current density was determined using a criterion of 1 μV/cm as the voltage drop across the voltage leads

TABLE A-8
SUMMARY OF THE PROPERTIES OF Y123 FILMS ON VARIOUS SUBSTRATES

	MIXED LIGAND PROCESS			COPPER (II) 2-ETHYLHEXANOATE PROCESS (2 EH)		
SUBSTRATE	YSZ	Ag	$SrTiO_3$ (100)	YSZ	Ag	$SrTiO_3$ (100)
ANNEALING	10 MIN AT 921°C 24 HR AT 405 °C	1 MIN AT 921°C 24 HR AT 405°C	10 MIN AT 903°C 31 HR AT 400°C	10 MIN AT 920°C 7 HR AT 400°C	3 HR AT 920°C 10 HR AT 400°C	<1 MIN AT 821°C 19 HR AT 400°C
T_c	$T_{50,\rho}$ = 91 K ΔT_ρ = 4 K	$T_{50,\chi}$ = 63 K ΔT_χ = 50 K T_{ONSET} = 88-90K χ_{fc}/χ_{zfc} = 0.5	$T_{50,\rho}$ = 86 K ΔT_ρ = 16 K	$T_{50,\rho}$ = 78 K ΔT_ρ = 20 K	$T_{50,\chi}$ = 63 K ΔT_χ = 50 K T_{ONSET} = 85-90K χ_{fc}/χ_{zfc} = 0.5	$T_{50,\chi}$ = 77 K ΔT_χ = 12 K
STRUCTURE	ORIENTED: ≤30[1] SUBMICRON CRYSTALLITES	ORIENTED: ≤20 SUBMICRON CRYSTALLITES	ORIENTED: 50 0.5 TO 2 MICRON CRYSTALLITES		ORIENTED: 200 FLAT ≤10 μm CRYSTALLITES	ORIENTED: 33 FINE GRAINS ~1 μm
J_c (G, 30 K)	300 A/cm^2					400 A/cm^2

1. ORIENTATION: $(I_{006}/I_{103})_{measured}/(I_{006}/I_{103})_{random\ oriented}$

J-762(12)
10-16-90

Two films with good superconducting properties were produced by the second processing method. X-ray diffraction measurements performed on these films showed a significant degree of c-axis orientation. Scanning electron microscopy on one of these films, dipped on a polycrystalline Ag substrate, revealed large (<10 μm) crystallites. Resistivity measurements of this film were not possible because of the high electrical conductivity of the Ag substrate. However, as shown in Fig. A-38, dc magnetic susceptibility revealed the onset of superconductivity between 85 and 90 K. The other film, $YBa_2Cu_3O_{7-\delta}$ dipped on a $SrTiO_3(100)$ substrate, was smooth with uniformly small grain size. Microprobe analysis on this film showed an excess of copper. Since the copper was not detectable by X-ray diffraction, we conclude that it may have existed in nano crystalline form in the intergranular region. While the reproducibility of this technique has not yet been demonstrated, the results are promising.

A.4. FLUX PINNING IN SOL-GEL DERIVED FIBERS OF DOPED $YBa_2Cu_3O_{7-\delta}$

A study of the effects of chemical dopants on the flux pinning properties of $YBa_2Cu_3O_{7-\delta}$ fibers is in progress. Fibers of $Y_{1-x}Pr_xBa_2Cu_3O_{7-\delta}$ and $Y_{1-y}Ce_yBa_2Cu_3O_{7-\delta}$ with varying concentrations ($0 \leq x \leq 0.10$; $0 \leq y \leq 0.01$) were prepared, and preliminary data on these systems have been obtained. Results on a series of $Y_{1-x}Pr_xBa_2Cu_3O_{7-\delta}$ fibers are as follows.

We believe that $Y_{1-x}Pr_xBa_2Cu_3O_{7-\delta}$ is an excellent candidate for flux pinning. Pr is the only rare earth element which forms the orthorhombic crystal structure $RBa_2Cu_3O_{7-\delta}$ (R = rare earth element but not Ce, Pm, or Tb) without exhibiting superconductivity. Resistivity measurements of $Y_{1-x}Pr_xBa_2Cu_3O_{7-\delta}$ ($\delta \sim 0.05$ (Ref. 23) indicate that T_c decreases monotonically for increasing Pr concentration x, as shown in Fig. A-39. Superconductivity vanishes for $x \sim 0.55$; however, for values of $x \leq 0.10$, T_c is depressed by no more than a few degrees.

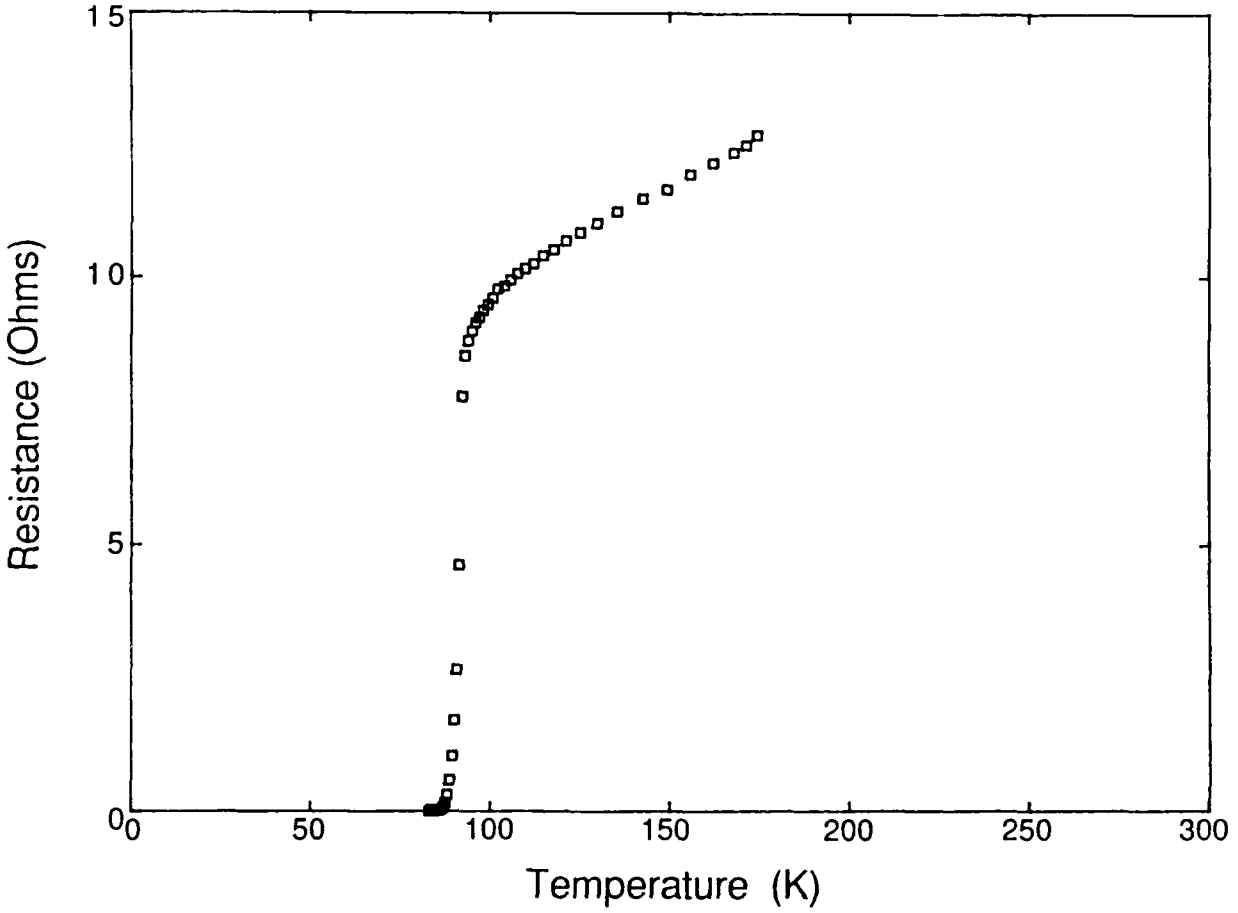

Fig. A-37. Resistivity as a function of decreasing temperature for an $YBa_2Cu_3O_{7-\delta}$ thin film on large-grained yttria-stabilized zirconia. The superconducting transition occurred with a midpoint at 91 K and a width of 4 K

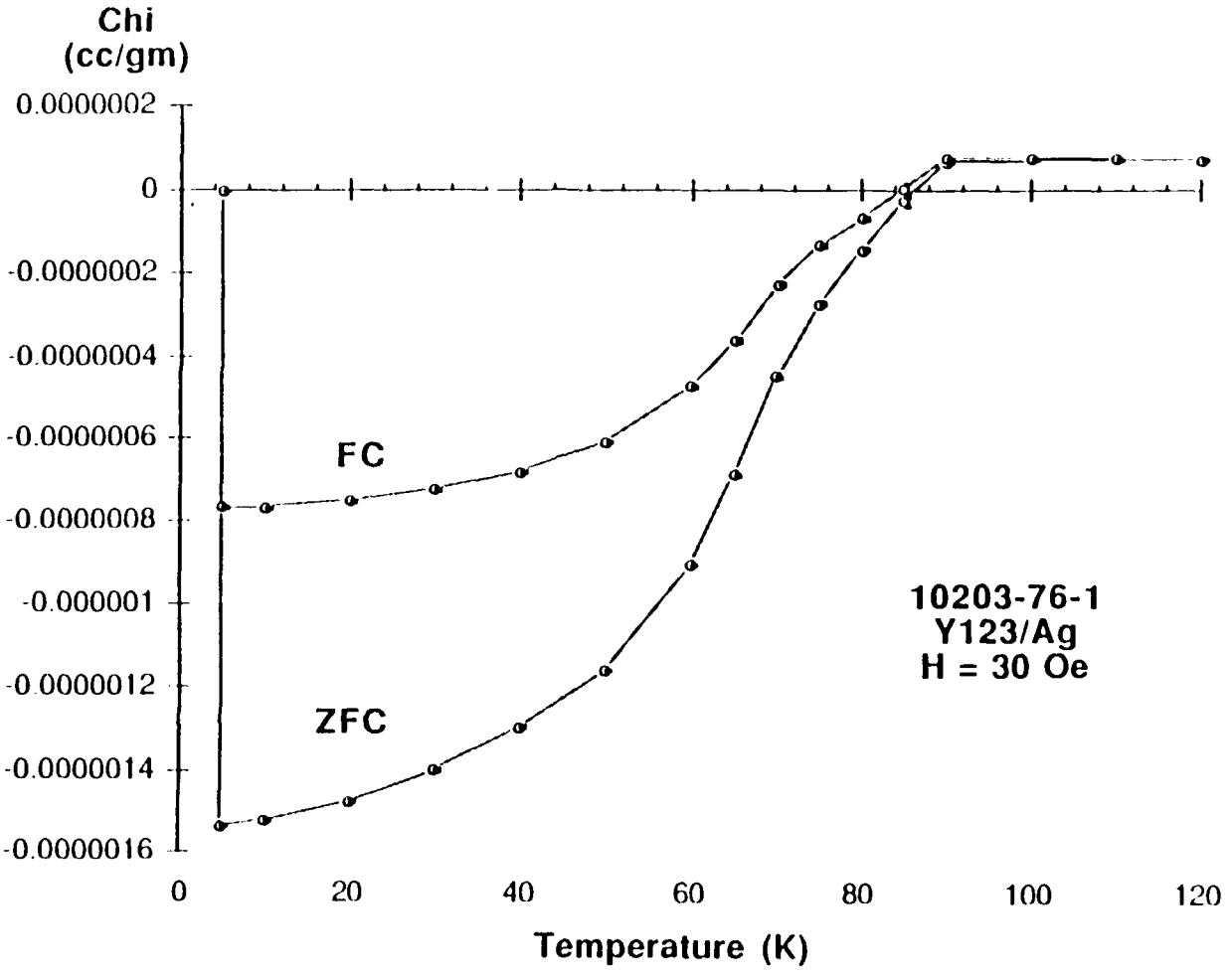

Fig. A-38. Magnetic susceptibility as a function of temperature for an $YBa_2Cu_3O_{7-\delta}$ thin film on polycrystalline Ag. The sample was cooled in zero field to 5 K, a field of 30 Oe was applied, and the sample was heated to 120 K and cooled to 5 K. The superconducting transition occurred with an onset above 85 K, a midpoint at 63 K, and a width of 52 K.

Fibers of $Y_{1-x}Pr_xBa_2Cu_3O_{7-\delta}$, x = 0, 0.0036, 0.05, and 0.10, were drawn and given identical heat treatments. Electron micrographs of the $Y_{0.9}Pr_{0.1}Ba_2Cu_3O_{7-\delta}$ sample, show a typical grain size of ~1 to 2 μm. Magnetic measurements were performed on these fibers in order to estimate the pinning energies and the intragranular critical current densities.

Magnetic relaxation data in Fig. A-40 were obtained by cooling the fibers in zero field to T = 30 K and subsequently applying a magnetic field of 5 kG. The magnetic moment of the sample was recorded at time intervals of 56 to 58 s beginning at t_0 = 290 s. The logarithmic time dependence of the magnetic moment is usually related to a thermally activated movement of flux lines through the sample (Ref. 24). If a single barrier height for the pinning centers is assumed, the magnetic moment M(t,T) can be calculated as (Refs. 25 and 26)

$$M(t,T) = M_0(T)\ [1 - (kT/U)\ \ln\ (t/\tau)] \quad , \qquad (A\text{-}1)$$

where $M_0(T)$ depends on the critical current in the absence of thermal fluctuations, U = U(T) is the pinning potential, and τ is the hopping time ($10^{-12} < \tau < 10^{-6}$ s). thus, the magnetization at a particular time t_0 is

$$M(t_0,T) = M_0(T)\ [1 - (kT/U)\ \ln\ (t_0/\tau)] \quad ,$$

which can be used to eliminate $M_0(T)$ from Eq. A-1. A plot of the normalized magnetization, $M(t,T)/M(t_0,T)$, as a function of ln t has a slope of S_n given by

$$S_n = [U/kT - \ln(t_0/\tau)]^{-1} \quad .$$

The magnetic relaxation data in Fig. A-41 indicate that flux pinning increases with increasing Pr concentration. Pinning energies U calculated from the slopes, plotted as squares in Fig. A-42, indicate a pinning potential more than 50% higher in the 10% Pr sample than in the

undoped sample. A typical error bar reflects the uncertainty in τ. The 0.36% Pr fibers were crushed and remeasured for flux relaxation; the pinning potential for the powder, plotted as a circle, was approximately 20% lower than for the fibers, indicating that some of the flux pinning probably occurs at the grain boundaries.

Magnetic hysteresis measurements were also performed on the fibers. Data for the undoped sample at T = 30 K, is shown in Fig. A-43. The intragranular critical current density can be estimated using Bean's critical state model (Ref. 27) and

$$J_c = F\Delta M/d \quad ,$$

where F is a geometrical factor such that F = 30 for a cylinder of diameter d, and $\Delta M = (M\downarrow - M\uparrow)$ is the magnetic hysteresis. The estimated critical current densities J_c are plotted in Fig. A-44, assuming the bulk density and an average grain size of d = 2 μm. Due to possible variations in the densities and grain sizes of the fibers, the values of J_c were normalized to their values in zero applied field, and these data are plotted in Fig. A-45. These results suggest that the field dependence of samples doped with Pr is improved over the undoped sample for H < 20 kG.

thus, the initial data indicate that $Y_{1-x}Pr_xBa_2Cu_3O_{7-\delta}$ is a promising candidate for increased flux pinning. Work in progress includes compositional studies by electron microprobe to confirm the Pr concentration and comparison between the fibers and samples prepared by solid state reaction. In addition, efforts are underway to improve the reproducibility of the transport critical current measurements.

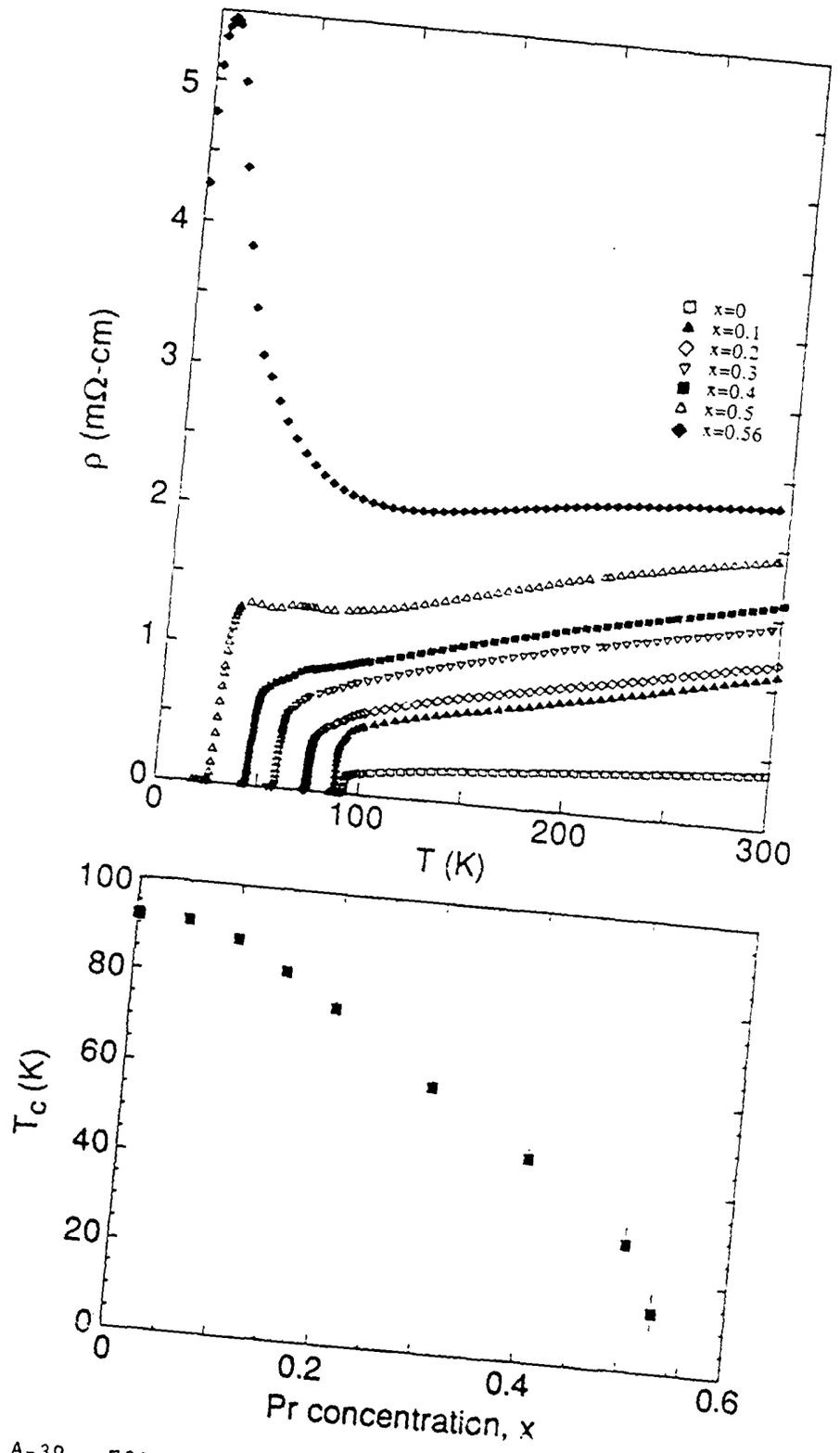

Fig. A-39. Effect of Pr concentration on transition temperature Tc (Ref. 23)

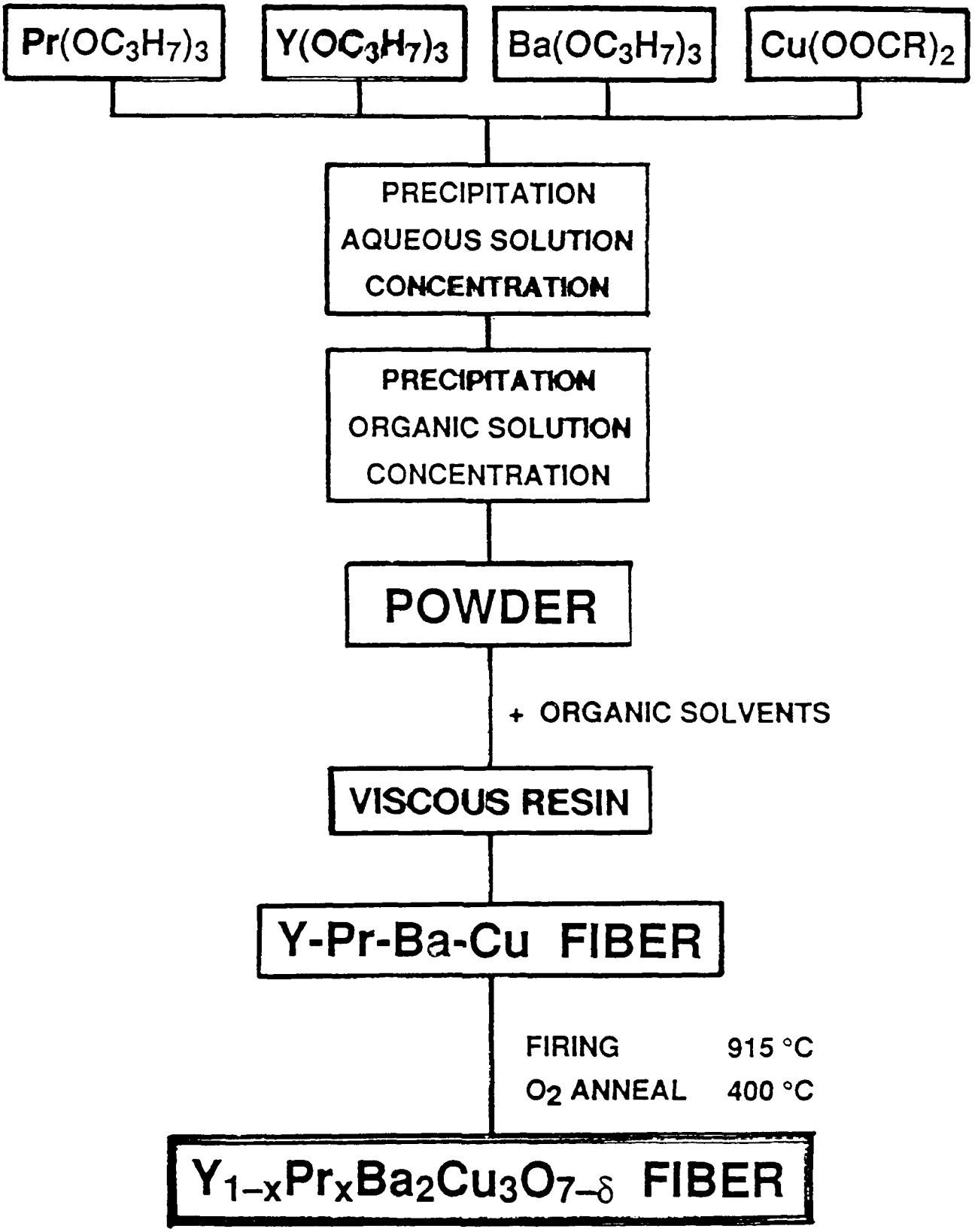

Fig. A-40. Flow diagram for adding Pr to the YBCO precursor compounds

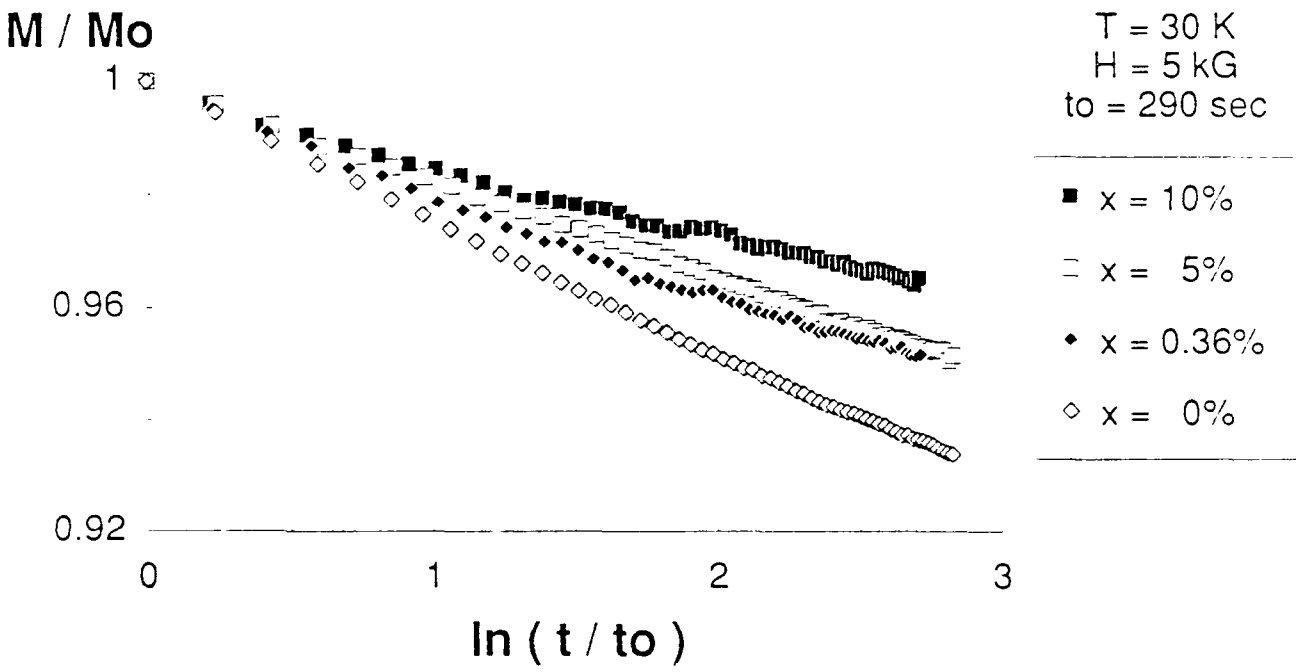

$$\frac{d\left(\frac{M}{M_o}\right)}{d\ lnt} = \left[ln\ \frac{t_o}{t} - \frac{U}{kT}\right]^{-1}$$

Fig. A-41. Magnetic relaxation

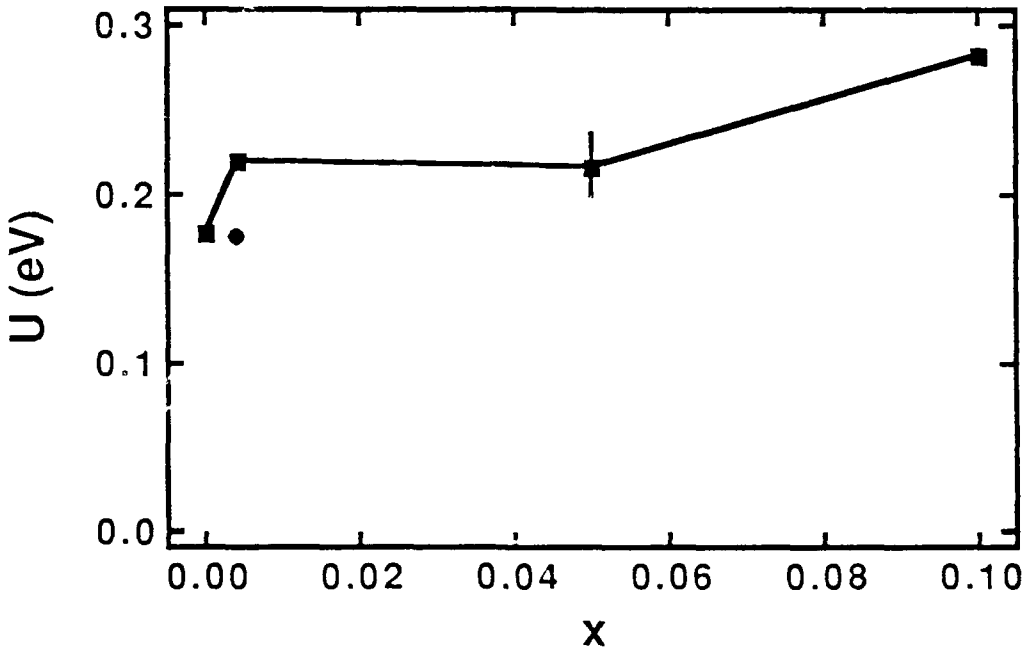

Fig. A-42. Pinning energy versus pr concentration

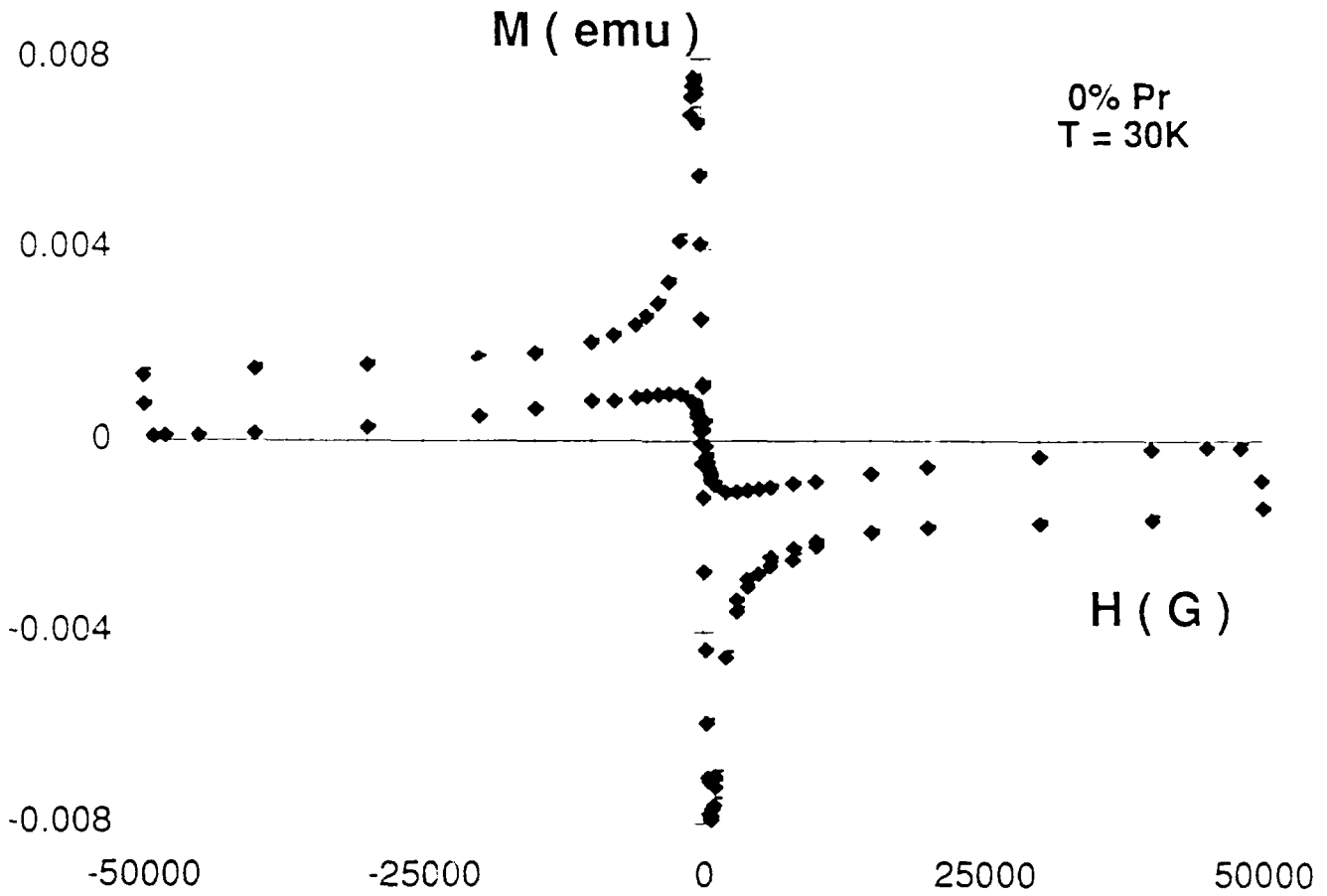

Fig. A-43. Magnetic hysteresis measurements using Bean's critical state model

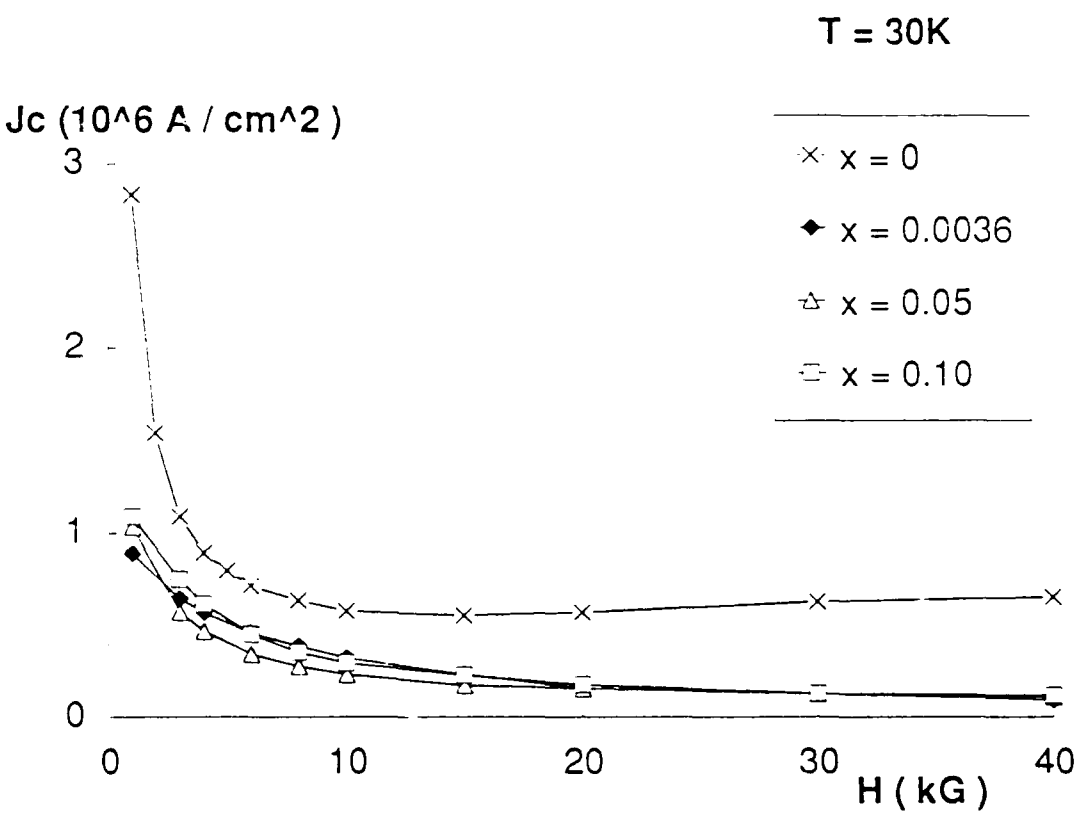

Fig. A-44. Estimated critical current densities J_c from Fig. A-43

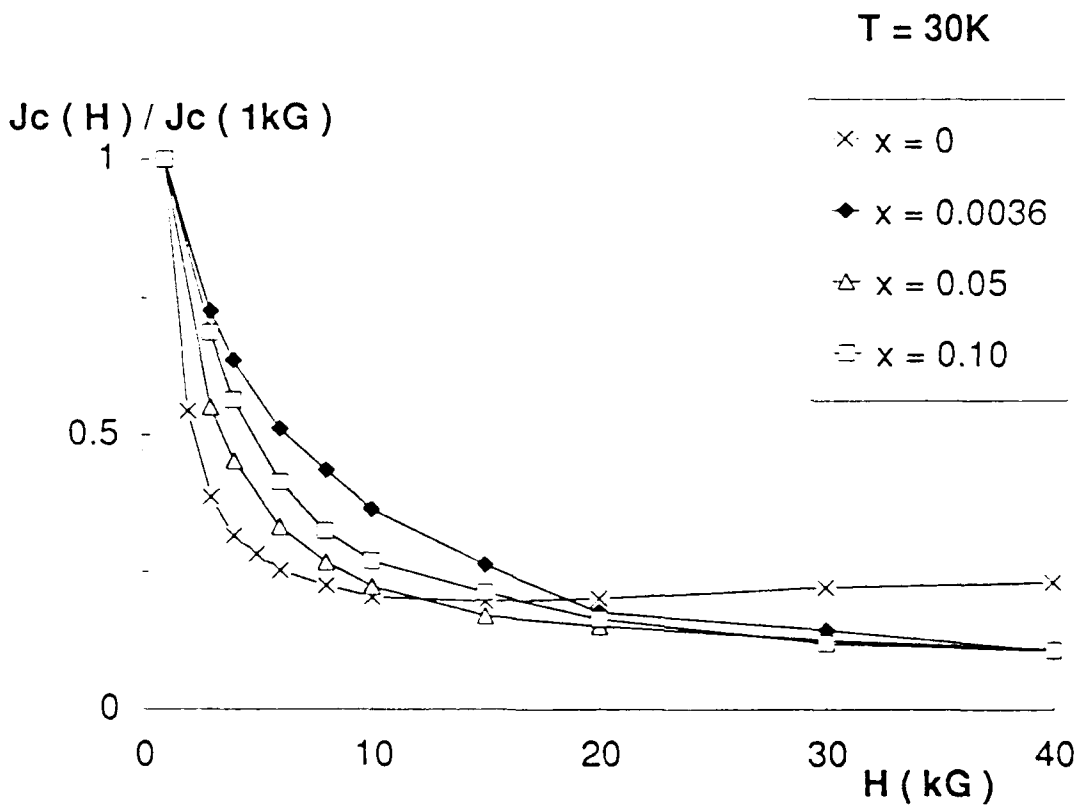

Fig. A-45. Normalized J_c in zero applied field

A-5. REFERENCES

1. Bedonrz, J. G., and K. A. Mullar, Z Phys., B64, 189 (1986).
2. Wu, M. K., I. R. Ashburn, C. J. Torng, D. H. Hor, R. L. Meng, L. Gao, Z. J. Huang, Y. Q. Wang, and C. W. Chu, Phys. Rev. Letter, 58, 908 (1987).
3. Subramanian, J. S. Science, 239, 1015 (1988).
4. Steng, Z. Z., et al., Phys. Rev. Letter, 60 (10), 937 (1988).
5. Worthington, T. K., W. J. Gallagher, and T. R. Dinger, Phys. Rev. Letter, 59, 1160 (1987).
6. Chandhari, P., R. H. Koch, R. B. Laibowitz, T. R. McGuire, and R. J. Cambino, Phys. Rev. Letter, 58, 2864 (1987).
7. Shi, D., D. W. Capone, II, G. T. Gaudy, J. P. Singh, N. J. Zaluzee, and K. C. Goretta, Mater. Lett., 6, 217 (1988).
8. Okada, M., A. Okayama, T. Morimoto, T. Matsumoto, K. Ahira, and S. Matsuda, Japan. J. Appl. Phys., 27, L185 (1988).
9. Barboux, P., J. M. Tarascon, L. H. Green, G. W. Hull, and B. G. Bagley, J. Appl. Phys., 63, 2725 (1988).
10. Wang, H. H., K. D. Carlson, U. Geiser, R. J. Thron, H. C. Kao, M. A. Beno, M. R. Monaghan, T. J. Allen, R. B. Proksch, D. I. Stupka, J. M. Williams, B. K. Flandermeyer, and R. B. Poeppel, Inorg. Chem., 26, 1474 (1987).
11. Dunn, B. C. T. Chu, L. W. Zhow, J. R. Copper, and G. Gruner, Adv. Ceram. Mater., Suppl. 2, 343 (1987).
12. Kordas, G., K. Wu, U. S. Brahme, T. A. Friedman, and D. M. Ginsberg, Mater. Lett., 5, 417 (1987).
13. Accibal, M. A., J. W. Draxton, A. H. Gabor, W. L. Gladfelter, B. A. Hassler, and M. L. Mecartney, "Better Ceramics Through Chemistry III," Edited by C. J. Brinker, D. E. Clark, and D. R. Ulrick (MRS Proc. Vol. 121).
14. Johnson, S. M., M. I. Gusman, D. J. Rowcliff, T. H. Gegalle, and J. Z. Sun, Adv. Ceram. Mater., 2, 337 (1987).
15. Kodas, T. T., E. M. Engler, V. Y. Lee, R. Jacowitz, T. H. Baum, K. Roche, S. S. P. Parking, W. S. Young, S. Hughes, J. Kleder, and W. Auser, Appl. Phys. Lett., 52, 1622 (1987).

16. Merkle, B. D., R. N. Kniseley, F. A. Schmidt, and I. E. Anderson, J. Mater. Sc. and Eng. (to be published).

17. Dole, S. L., O. Hunter, Jr., F. W. Calderwood, and D. J. Bray, J. Am. Ceram. Soc., 61, 486 (1978).

18. Shaw, T. M. S. L. Shinde, D. Dimos, R. F. Cook, P. R. Duncombe, and C. Kroll, J. Mat. Research, Vol. 4, No. 2, 248-256 (1989).

19. Fahrenholtz, W. G., D. M. Miller, and D. A. Payne, "Preparation of $YBa_2Cu_3O_{(7-x)}$ from Hommogeneous Metal Alkoxide Solution," Advanced Ceramic Materials, preprint.

20. Mazdiyasni, K. S., et al., "High Temperature Ceramic Superconductors for Period January 1, 1990-March 31, 1990," General Atomics Report GA-C19465, April 10, 1990.

21. Naito, M., et al., J. Material Research, 2(6), 713 (1987).

22. Cheung, C. T., and E. Ruckenstein, "Superconductor-Substrate Interactions of the Y-Ba-Cu Oxide," J. Materials Research, 4(1), 1 (1989).

23. Neumeier, J. J., Ph.D. Thesis, University of California, San Diego, 1990.

24. anderson, P. W., Phys. Rev. Lett., 9, 309 (1962).

25. Hagen, C. W., R. P. Griessen, and E. Salomons, Physica C, 157, 199 (1989).

26. Tinkham, M., and C. J. Lobb, Solid State Physics, 42, Eds. H. Ehrenreich and D. Turnbull, Academic Press, new York, 1989.

27. Bean, C. P. Phys. Rev. Lett., 8, 250 (1962).